MICROCOPY RESOLUTION TEST CHART

NATIONAL BUREAU OF STANDARDS 1963 A

AD A138064

DTIC

①
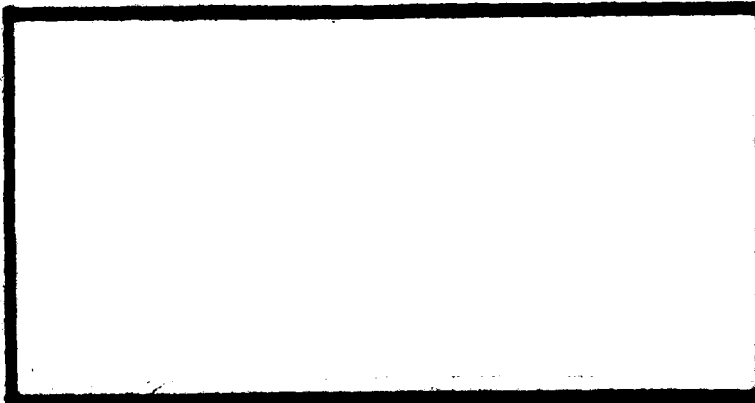
DTIC
ELECTE
FEB 2 2 1984
S          D
          B

**DEPARTMENT OF THE AIR FORCE**
**AIR UNIVERSITY**
# AIR FORCE INSTITUTE OF TECHNOLOGY

Wright-Patterson Air Force Base, Ohio

84 02 21 188

IMPLEMENTATION AND EVALUATION

OF TWO DESIGN CONCEPTS OF THE

PASSIVE RING RESONATOR LASER GYROSCOPE

THESIS

AFIT/GEO/EE/83-3 Mark E. Nelson
Captain USAF

DTIC
ELECTE
FEB 2 2 1984
S D
B

IMPLEMENTATION AND EVALUATION

OF TWO DESIGN CONCEPTS OF THE

PASSIVE RING RESONATOR LASER GYROSCOPE

THESIS

Presented to the Faculty of the School of Engineering

of the Air Force Institute of Technology

Air University

in Partial Fullfillment of the

Requirements for the Degree of

Master of Science

by

Mark E. Nelson, B.S.

Capt                    USAF

Graduate Engineering Physics

December 1983

## Preface

The purpose of this study was twofold: to compare the relative merits of two designs of the passive ring laser gyroscope, and to determine the performance level possible using a high finesse low noise resonant cavity. The rotation sensitivities measured in this research indicate that the passive ring laser gyroscope can match and possibly surpass current performance levels of active laser gyroscopes.

I would like to thank Major Salvatore R. Balsamo, first and foremost, as the prime mover behind this research. I would also like to thank Rockwell International for providing the resonant cavity that made this research possible, and the personnel of the F.J. Seiler Research Laboratory for their sponsorship and tremendous support. In particular, I wish to express my sincere appreciation to Major Gerry Shaw who gave both his time and equipment to insure the successful completion of this research, and to his assistant, 2Lt. Frank Rand, for the many hours he spent in aligning the gyro for the first data measurements.

Of course, I must thank my wife, Lila, for countless things, but mainly for her love, devotion, and sacrifices that enabled me to pursue this research, and my family and friends for their continued love and support.

Mark E. Nelson

# Table of Contents

# List of Figures

## List of Figures

## List of Figures

## List of Tables

## Abstract

Two configurations of the passive resonant ring laser gyroscope were evaluated. The first configuration detected cavity resonance by monitoring the beams transmitted through the cavity. The second configuration detected resonance by monitoring the beams reflected from the cavity input mirrors. The resonant cavity of both configurations had a rated finesse of 9800, making the gyro much more sensitive than earlier versions. Additionally, much of the cavity noise that plagued earlier experiments was eliminated by mounting the cavity mirrors on a solid ceramic block, and evacuating the beam paths.

Alignment data indicated that the signal strength in the reflected beam had six times the power of the signal in the transmitted beam. However, the bias on the reflected signal was seven times the signal strength. This bias intensity increased the shot noise in the detector circuit.

Rotation was simulated in the gyro by shifting beam frequencies. The strength of the error signal was calibrated to angular rotation. A signal to noise ratio of one was then converted to a noise equivalent rotation. Using a 100 second integration time, the noise equivalent rotation of the first configuration was twelve milli-earthrate, and four milli-earthrate for the second configuration. The detection of resonance using the reflected beam increased sensitivity threefold.

# I. INTRODUCTION

## Background

The ring laser gyroscope first appeared in a working
form in 1963 when Macek and Davis built a working model based
on an earlier design by Rosenthal. In 1972 the first opera-
tional model was available. Currently the ring laser gyro is
used for rotation sensing in inertial platforms as an alter-
native to the mechanical gyro, as in the Boeing 757. The ring
laser gyro has distinct advantages over the mechanical gyro
such as a fast warm up time and few moving parts to wear out.
It is also free of many of the errors associate with mechan-
ical gyros. Laser gyros, however, have their own characteris-
tic errors of which the most significant is a lock-in error
at low rotation rates. This lock-in error is primarily due to
the laser gain medium in the ring laser gyroscope.

In 1977, Balsamo and Ezekiel proposed using an external
laser source to eliminate this lock-in error. In 1978, two
AFIT students, Olkowski and Holland, under the tutelage of
Balsamo, built and tested a Passive Ring Laser Gyroscope
(PRLG). In 1979, Motes carried on the study of Olkowski and
Holland by building a second version in an attempt to elim-
inate the error sources in the previous design.

In both models, the largest errors were caused by the
instability of the resonant cavity. Because the cavity com-
ponents were individually mounted on a platform base, the
quality of the cavity was severely limited. The major error
sources were: (1) the thermal expansion of the cavity and the

associated misalignment of the cavity, (2) the mechanical
vibration of the cavity mirrors by platform vibrations and
air currents, and (3) the variation of the index of refraction within the cavity due to vibrations and air currents.

## Problem Statement

The primary objective of this research is to compare
the performance of two design concepts of the PRLG. The
first design concept has been used in previous PRLG's. It
consists of monitoring the power transmitted through the cavity to keep the two cavity beams in resonance. The second
design concept differs from the first in that the power reflected from the cavity is monitored to keep the two cavity
beams in resonance. Since the principle function of the PRLG
is to accurately measure rotation, rotation rate sensitivity
is the performance factor used to compare the two designs.

A second, but equally important objective, is to maximize the rotation rate sensitivity in either design to the
performance level of one milli-earthrate (0.015041 deg/hr).
Although the rotation rate sensitivity in previous PRLG's
has been much coarser than milli-earthrate, the quality of
the resonant cavity makes this a conceivable goal. The Rockwell International cavity used in this research is drilled
from a solid piece of "Zerodur", a ceramic, one of the most
thermally stable materials known. The piezo-electric transducers and cavity mirrors are attached directly to the "Zerodur" block and aligned to sustain a gaussian beam. Each mirror consists of 23 dielectric layers on a "Zerodur" substrate

finished to a smoothness of less than 0.5 Å. The reflecti-
vity for the mirrors at 6328Å is 0.99995. The cavity is par-
tially evacuated to reduce variations in index of refraction
within the cavity. These qualities of the resonant cavity
eliminate the dominate noise source of earlier versions of
the PRLG, and increase the resolving power by a factor of
fifty. Hence, a goal of milli-earthrate is realistic. (Ref 1)

Finally, the development of the PRLG will, most likely,
continue to be a source of AFIT theses. The third objective
of this thesis is to provide a comprehensive background in
PRLG theory that will aid future AFIT research.

## Scope

The scope of the research is limited to the design, fab-
rication, testing, and evaluation of two configurations of
the PRLG. Two major components of the PRLG, the resonant cav-
ity and the frequency stabilized laser, are treated as com-
pleted components. The primary design feature in this re-
search is mode matching. The first configuration tested was
designed by Majors Balsamo and Shaw. The second configuration
tested is designed in this research.

## General Approach

A PRLG is designed which utilizes the first concept of
resonant peak detection, monitoring power transmitted through
the cavity. The primary design feature is mode matching the
gaussian beam of the frequency stabilized laser to the mode
supported by the cavity. The geometry of the first configura-

tion allows an approximate mode match by the use of two spherical mirrors. Once the design is completed, the laser, acousto-optics, beamsplitter, mirrors, and cavity are mounted on an "Invar" base, and aligned. Measurements are recorded to determine cavity finesse, and rotation rate sensitivity. At the completion of the first test, the PRLG is dismantled. Some mounts are replaced and the PRLG is realigned in the same configuration for a second series of tests. A second set of data is recorded.

Next, a PRLG is designed which detects resonance from the reflected cavity beam. The modes of the laser and cavity are matched using two spherical lenses. The components are mounted on a stainless steel base and aligned. Data measurements are again recorded to determine cavity finesse and rotation rate sensitivity. At the completion of the first test in the second configuration, the PRLG is realigned to maximize finesse. The gain in the electronic feedback loops is maximized. A final set of data is taken. Additionally a recording of bias drift over a 30 minute period is accomplished for this configuration.

## Order of Presentation

Chapter II presents the general theory of rotation sensing using optical components. This chapter is subdivided into six sections: (1) the Sagnac effect, (2) optical cavities, (3) the active ring laser gyroscope, (4) the passive ring laser gyroscope, (5) acousto-optic modulators, and (6) mode matching. Chapter III presents the two configurations of the

PRLG to be tested, briefly describes the mode matching, and discusses the specifications of the resonant cavity. Chapter IV descibes the data measurements taken and presents the data. Chapter V discusses the data, compares the two configurations, and gives conclusions and recommendations.

## II. THEORY

### The Sagnac Effect

The Sagnac effect is the basic principle behind all ro-
tation sensing using light. It refers to the shift in opti-
cal path-length that occurs in a ring cavity when it is ro-
tated. This shift occurs as a result of the relativistic law
that the speed of light is a constant in a given inertial
reference frame.

Consider the following example: a ring cavity consist-
ing of three mirrors, Fig. 1, is rotated in the clockwise
direction. To an observer A, who is stationary in the iner-
tial reference plane, the speed of the light traveling in the
clockwise (cw) and counter-clockwise (ccw) direction is the
constant c. But to observer B, who is in the reference plane
of the rotating ring, the light traveling in the cw direction
appears to be traveling slower than c, while the light tra-
veling in the ccw direction appears to be traveling faster
than c. In each case the apparent speed is equal to the con-
stant speed of light, c, plus or minus the peripheral velo-
city of the ring, $R\Omega$, where $\Omega$ is the angular velocity in ra-
dians per second and R is the radius from the center of ro-
tation to the light beam. To observer A, the light traveling
in the cw direction from point D must travel farther than the
ccw beam to arrive back at point D, since as the beams tra-
vel, point D moves away from the cw beam and toward the ccw
beam.
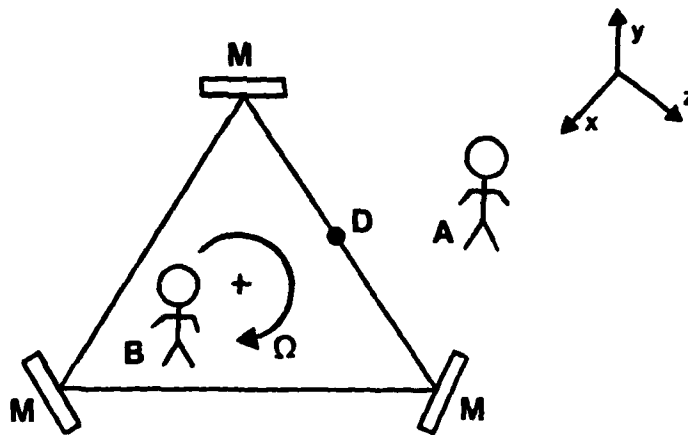
Fig. 1. The Sagnac Effect

The difference in path length can be computed by multiplying the difference in peripheral velocity, $2R\Omega$, by the time that the light takes to complete one round trip. Since the speed of light is much much greater than the peripheral velocity in practical devices, the round trip time is well approximated by the perimeter of the light path divided by the constant speed of light, c.

For a circular ring the radius of the light path from the center of rotation is constant, the peripheral velocity of the ring ($R\Omega$) is constant, and the perimeter of the light path is the perimeter of a circle ($2\pi R$). Then the path length difference, $\Delta L$, is:

$$\Delta L = \Delta v \times t$$
$$= 2R\Omega \times 2\pi R/c$$
$$= \frac{4\pi R^2}{c} \Omega \qquad (1)$$

For a noncircular light path as shown in Fig. 2, the radius changes as a function of $\theta$, so the path length difference must be integrated around the loop:

$$\Delta L = \int_0^{2\pi} \frac{2R^2\Omega}{c} \, d\theta \qquad (2)$$

where;   $\Delta L$ = the total path length difference

$2\Omega R$ = the difference in angular velocity at each point along the path

$Rd\theta$ = the incremental path length at each point that is tangent to the axis of rotation

$R$ = a variable radius that is some function of $\theta$

Moving the constants outside of the integral, Eq (2) becomes;

$$\Delta L = \frac{2\Omega}{c} \int_0^{2\pi} R^2 \, d\theta \qquad (3)$$
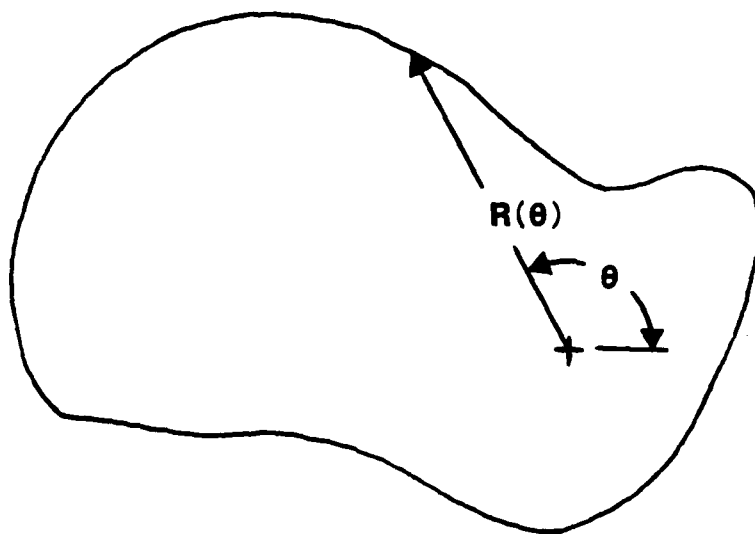


Fig. 2.   An Irregular Optical Path

II-3

The integration of $R^2$ over $\theta$ is equivalent to twice the area that the radius sweeps out as it is integrated. So when $\theta$ is integrated from 0 to $2\pi$, the radius sweeps the entire area that is enclosed by the light path, and the product of the integrand is simply $2A$. This relationship between $R^2$, $\theta$, and $A$ is best illustrated by replacing the integration with a summation, Fig. 3, of many small wedges, $\Delta\theta$:

$$\Delta L = \frac{2\Omega}{c} \sum_{i=1}^{n} R^2 \Delta\theta \tag{4}$$

In each wedge $\Delta\theta$, the radius can be approximated as the average radius. Then the incremental area enclosed by each
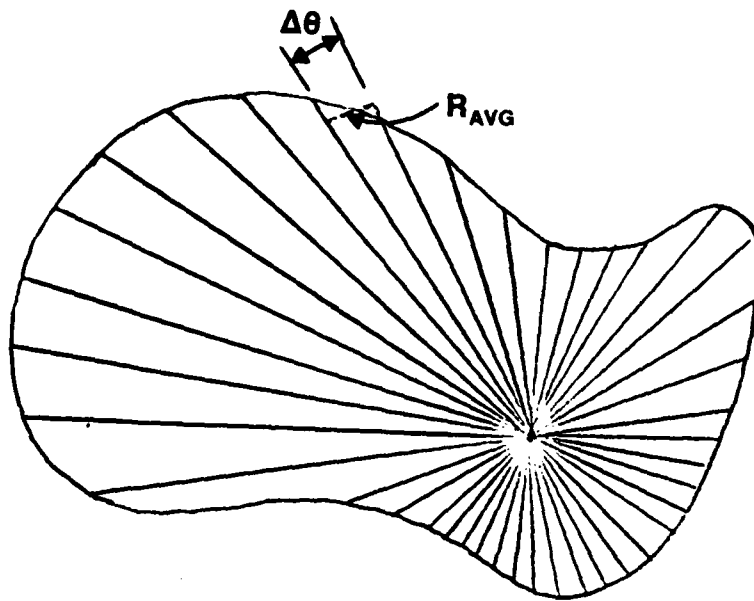


Fig. 3.  Path Length Difference as a Summation

wedge is:

$$\Delta A = \frac{R^2}{2} \Delta\theta \qquad (5)$$

where $\Delta\theta$ is in radians. So:

$$R^2 = \frac{2\Delta A}{\Delta\theta} \qquad (6)$$

By substituting Eq (6) into Eq (4), the summation becomes:

$$\Delta L = \frac{2\Omega}{c} \sum_{i=1}^{n} \frac{2\Delta A}{\Delta\theta} \Delta\theta \qquad (7)$$

By factoring 2 out of the summation and cancelling $\Delta\theta$,
Eq (7) becomes:

$$\Delta L = \frac{4\Omega}{c} \sum_{i=1}^{n} \Delta A \qquad (8)$$

which is simply the summation of incremental areas which add
up to the total area enclosed. By taking the limit as $\Delta\theta \rightarrow 0$,
the errors caused by the approximation of radius disappear,
and the summation becomes the integration of area enclosed by
the beam path:

$$\Delta L = \frac{4\Omega A}{c} \qquad (9)$$

This result is valid no matter what geometry the beam
path takes, or where the center of rotation is located. The
only assumption·made in deriving Eq (9) is that the speed of
light is much much greater than the peripheral velocity of
the ring.

## Optical Cavities

An optical cavity is any configuration in which light travels a closed path. The simplest optical cavity is the Fabry-Perot etalon, Fig. 4, which consists of two parallel fixed mirrors separated by some distance L. Light reflects back and forth between the mirrors A and B forming a closed path of length 2L. Many properties of all cavities can be defined in terms of this simple configuration.

Consider first the characteristic modes of an optical cavity. In general, a cavity mode is any wave shape that reproduces itself after one round trip through the cavity, that is, it has the same phase and electric field distribution. There can be more than one such wave for a given cavity, and each is a characteristic mode. The curvature of the cavity mirrors and the geometry of the cavity determine the characteristic modes. Modes are discussed in more detail in the last section of this chapter.
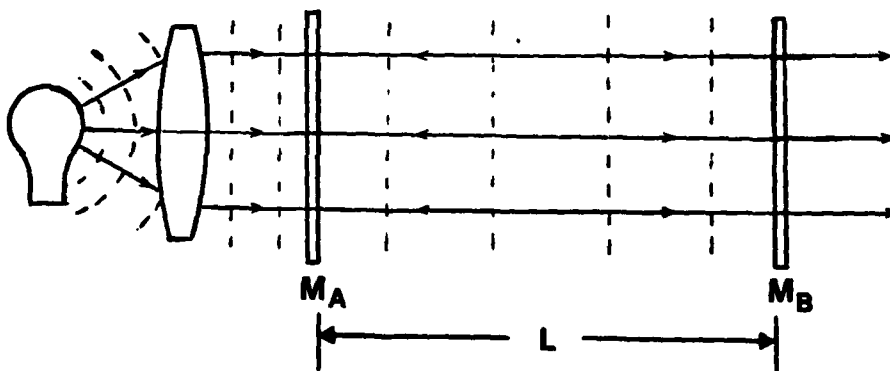


Fig. 4.   Fabry-Perot Etalon

Resonance is another property of optical cavities. Consider a beam of light entering the cavity of Fig. 4 through mirror A. The beam propagates to mirror B where part of the beam is transmitted and part is reflected back to mirror A after traveling a distance of 2L. For the cavity to be in resonance, the reflected beam must be in phase with the beam just entering the cavity. This phase match occurs when the round trip length through the cavity is an even number of wavelengths: $2L = n\lambda$, where $\lambda$ is the wavelength of the light and n is any integer. This condition is necessary for constructive interference.

The resonance relationship can also be expressed in terms of frequency by substituting $c/f$ for $\lambda$, where f is frequency in Hz. Solving for f, the resonance equation becomes;

$$f = \frac{nc}{2L} \qquad (10)$$

Frequencies that satisfy Eq (10) are called resonant frequencies of the cavity. The distance between resonant frequencies is called the Free Spectral Range (FSR) of the cavity. From Eq (10) it is obvious that the FSR must be $c/2L$.

In a perfect cavity where the mirrors are 100% reflective, each reflected wave has the same amplitude as the original wave. If the cavity is not exactly in resonance then the reflected wave is not perfectly in phase with the source wave. The second and third reflection are two and three times out of phase and so on until the phase of the $n^{th}$ reflected wave is shifted a full wavelength and is again in phase with

the source. The net effect of the interference of all re-
flected waves is total destructive interference.

In a real cavity, the reflected beam diminishes in am-
plitude with each reflection so that at frequencies near re-
sonance, total destructive interference does not occur. In
this situation the reflected beams attenuate before they
phase shift a full wavelength.

When the cavity is in resonance, maximum power is trans-
mitted through the cavity. This property is a result of the
boundary conditions at the input mirror of the cavity.

Consider the boundary conditions shown in Fig. 5, where
a beam of light is incident on a highly reflective mirror.
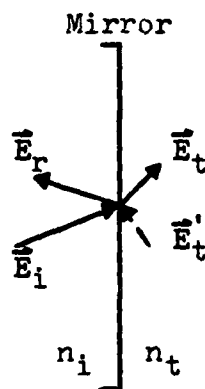
Mirror



Fig. 5. Boundary Conditions at the Cavity Input Mirror

The boundary conditions at the surface of the mirror result
in a portion of the wave being transmitted and a portion re-
flected. But when the mirror is part of a cavity in reson-
ance, a fourth component is added to the boundary condition,

which is the reflected cavity wave $\overline{E}_t'$. The returning cavity wave's $\overline{E}_t'$ cancels a portion of the reflected wave's $\overline{E}_r$ resulting in an increase in the transmitted wave's $\overline{E}_t$. The increased transmitted beam in turn increases the returning cavity beam, and the process iterates until the boundary conditions are stable. If the reflectivity of the other cavity mirrors accumulatively match the reflectivity of the input mirror, then the three components $\overline{E}_i$, $\overline{E}_t$, and $\overline{E}_t'$ completely match the boundary conditions and no light is reflected.

The formula for transmission through an optical cavity in resonance is:

$$T = \frac{(1-R_1)\ (1-R_2)}{\left[1 - (R_1 R_2)^{\frac{1}{2}}\right]^2} \qquad \text{(Ref 7:116)} \qquad (11)$$

where

$T$ = portion of incident power transmitted

$R_1$ = reflectivity of the input mirror

$R_2$ = combined reflectivity of other cavity mirrors

As the frequency shifts away from the resonant frequency, destructive interference begins in the reflected waves. $\overline{E}_t'$ no longer phase matches $\overline{E}_t$, $\overline{E}_i$, and $\overline{E}_r$, and power transmitted falls off. Figure 6 shows a graph of proportional power transmitted through the cavity as a function of frequency.
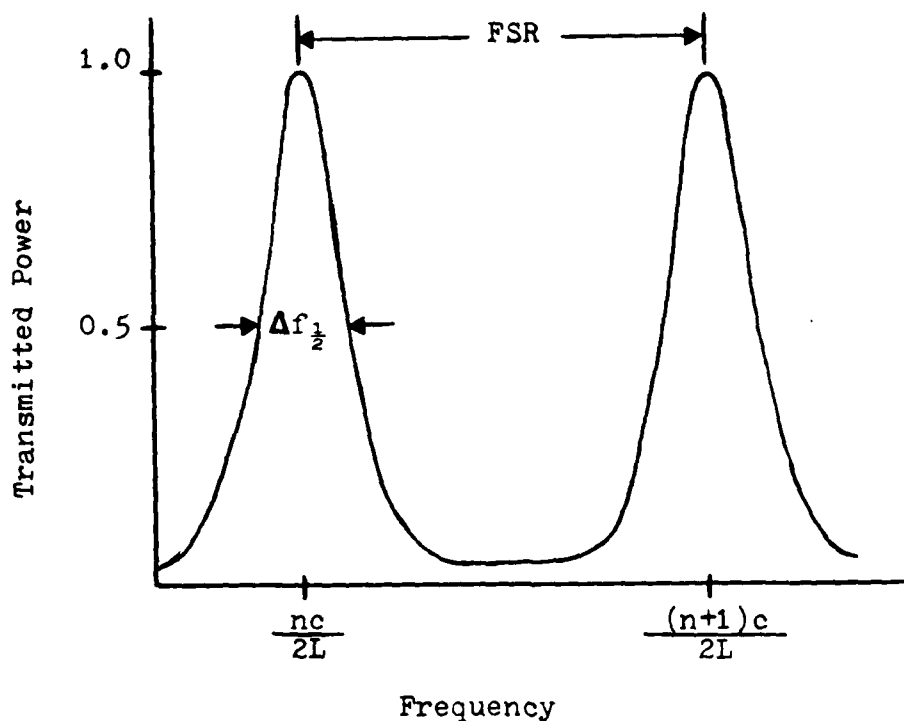
Fig. 6.  Cavity Power Transmission vs. Frequency

The higher the reflectance of the cavity mirrors, the faster the power falls off with frequency, and the narrower the resonant peak. The difference in frequency between half power points of the resonant peak is denoted by $\Delta f_{\frac{1}{2}}$, which stands for full width half maximum frequency. The $\Delta f_{\frac{1}{2}}$ in a lossless cavity is related to the reflectivities of the cavity mirrors by the following formula:

$$\Delta f_{\frac{1}{2}} = \frac{c}{2L} \; \frac{1-(R_1 R_2)^{\frac{1}{2}}}{\pi(R_1 R_2)^{\frac{1}{4}}} \qquad \text{(Ref 7:118)} \qquad (12)$$

The $\Delta f_{\frac{1}{2}}$ and FSR are two characteristics of an optical cavity that determine a third called the finesse of a cavity. The finesse is the number of $\Delta f_{\frac{1}{2}}$'s that would fit into one

II-10

FSR:

$$\text{finesse} = \frac{n(R_1 R_2)^{\frac{1}{4}}}{1-(R_1 R_2)^{\frac{1}{2}}} \qquad (\text{Ref } 7:118) \qquad (13)$$

The finesse is a measure of the resolving power of the cavity, that is, its ability to resolve one frequency of light from another within the same FSR. For most cavities the $\Delta f_{\frac{1}{2}}$ and hence the finesse are determined primarily by the reflectivity of the cavity mirrors as in Eqs (12) and (13). But when cavities have highly reflective mirrors, as in a laser cavity, the spatial distortion of the cavity beam becomes the dominant effect in shaping the resonant peak. Spatial distortion of the beam refers to the phase distortion of the wave as a result of reflection from an imperfect surface, as illustrated in Fig. 7.



Exaggerated
Mirror Surface
---- ideal
—— real

Incident
Wave
(Phase front)

Reflected
Wave
(Phase front)
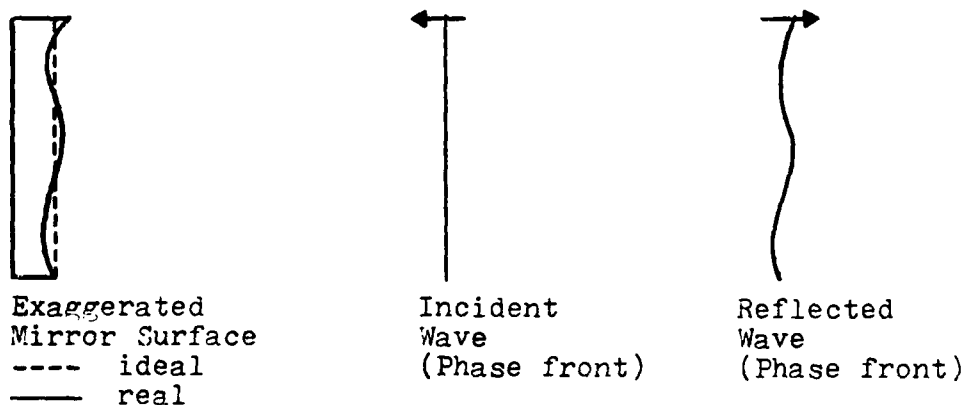
Fig. 7.  Spatial Phase Distortion of the Reflected Wave

The real surface of the mirror does not perfectly correspond to the desired surface, but varies higher and lower. When a perfect wave front is reflected from this surface, part of the wave is reflected from the high surface and part from the low surface. The spatial distortion of the wave phase is directly related to the spatial variation in the mirror surface. And the minimum $\Delta f_{\frac{1}{2}}$ and maximum finesse are directly related to the spatial distortion. The root mean squared (RMS) variation in the surface of the mirror expressed in wavelengths roughly corresponds to the inverse of the cavity finesse. So if the smoothness of the mirror were $\lambda/200$ the maximum finesse would be 200 no matter how reflective the mirrors were made.

When the resonant peak of the reflectivity is much narrower than the resonant peak of spatial distortion, then even in perfect resonance, much of the light wave is shifted so that destructive interference occurs. So, besides limiting the finesse of the cavity, spatial distortion of the phase front also limits the power that can be transmitted through the cavity.

The characteristics of the Fabry-Perot etalon are easily extended to the more complex cavity of Fig. 1. For resonance and FSR, the round trip is the perimeter, P, of the cavity. Eq (10) becomes:

$$f = \frac{nc}{P} \tag{14}$$

The reflectance of the input mirror of Fig. 1 corresponds to $R_1$ in Eqs (11),(12), and (13). Similarly the combined reflectance of mirrors 2 and 3 correspond to $R_2$. Equations (11), (12), and (13) become;

$$T = \frac{(1-R_1)\ (1-R_2 R_3)}{\left[1\ -\ (R_1 R_2 R_3)^{\frac{1}{2}}\right]^2} \tag{15}$$

$$\Delta f_{\frac{1}{2}} = \frac{c}{P}\ \frac{1-(R_1 R_2 R_3)^{\frac{1}{2}}}{(R_1 R_2 R_3)^{\frac{1}{4}}} \tag{16}$$

$$\text{finesse} = \frac{(R_1 R_2 R_3)^{\frac{1}{2}}}{1-(R_1 R_2 R_3)^{\frac{1}{4}}} \tag{17}$$

Similarly, for a four element cavity $(R_2 R_3)$ in Eqs (15), (16), and (17) would become $(R_2 R_3 R_4)$ and so on.

## The Active Laser Gyroscope

A laser can be viewed as three distinct components:
(1) a resonant optical cavity, (2) a gain medium, and (3) a pumping mechanism to excite the gain medium. Of these three components it is the resonant cavity of the laser gryoscope that makes it distinct from other lasers. Consider first those components common to other lasers.

The gain medium most often used in laser gyroscopes is Helium-Neon (HeNe) gas. The pumping mechanism for HeNe lasers is an electrical discharge through the gas. The electrons raise the Helium atoms to a higher energy state by collisions,

and the Helium atoms in turn raise the Neon atoms to a high-
er energy state. When sufficient Neon atoms are in the upper
state, the gain medium has the property of amplifying light
which falls in the narrow frequency range around the wave-
length of 6328 Å. This occurs because a photon of 6328 Å
light stimulates the Neon atom to emit an identical photon
of light. If the gain through the gas is greater than the
other losses in the cavity, then lasing occurs. Lasing con-
tinues as long as there are sufficient excited Neon atoms to
produce a gain greater than the cavity losses. In a contin-
uous-wave laser such as the HeNe, the lasing stabilizes at
a beam power such that the pumping mechanism is replenishing
upper state Neon atoms at the same rate that the lasing pro-
cess and other loss mechanisms are depleting them. A graph
of gain, $\gamma$, versus frequency, f, as shown in Fig. 8, for the
light amplification by the gain medium is called a gain pro-
file.

As shown in Fig. 8, the gain medium produces gains
greater than the cavity losses only for light within the
narrow frequency range from point A to point B. The resonance
of the optical cavity further restricts the frequency range
of lasing to be a multiple of $c/P$. By the nature of the las-
ing physics, light at the resonant frequency which has the
lowest cavity losses, undergoes the greatest amplification
until it is the only frequency amplified and non-resonant
frequencies die out. Thus the output frequency of the laser
is the resonant frequency of the laser cavity.
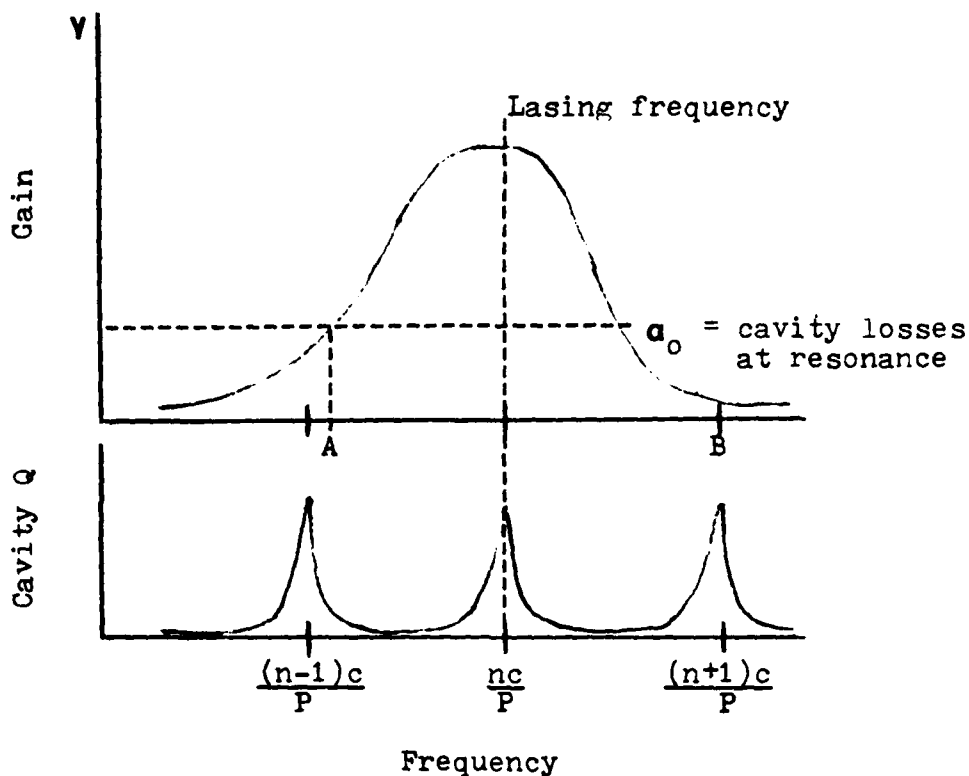
Fig. 8. HeNe Gain Profile and Resonance Condition

A laser gyroscope, also called a ring laser, is formed by chosing a Sagnac interferometer as the resonant optical cavity, Fig. 9. The ring laser is actually two lasers sharing the same gain medium. The cw and ccw paths of the resonant ring are independent of each other. The resonance of the cw and ccw paths is determined by their respective path length. So when a path length difference between the two is induced by rotation, the frequencies of the resonant peaks also shift.
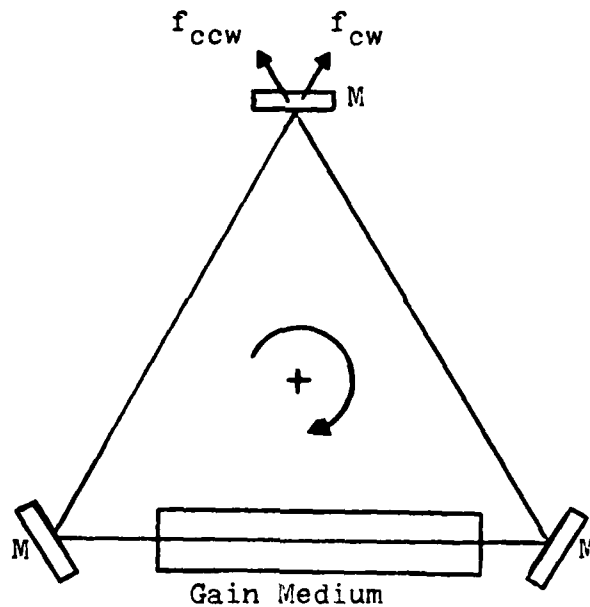
Fig. 9.   The Ring Laser

Consider a cw rotation of the ring laser in Fig. 9. The
angular rotation effectively changes the path length of the
cw and ccw paths by $\Delta L/2$, i.e. the Sagnac effect. This in-
crease in path length of the cw path then causes the resonant
frequency of that beam to decrease, while the decrease in
path length of the ccw beam causes the resonant frequency of
that beam to increase. This effect is apparent from Eq (14),
the resonant frequency is inversely proportional to the path
length. Because the change in both frequency and path length
caused by the Sagnac effect is very small compared to the
initial frequency and path length, the proportional changes
in both are essentially equal:

$$\frac{\Delta f}{f} = \frac{\Delta P}{P} \qquad (18)$$

Since $\Delta P = 4A\Omega/c$, and $f = c/\lambda$, these values can be substituted into Eq (18). Solving for f;

$$\Delta f = \frac{4A}{P\lambda}\,\Omega \qquad\qquad (19)$$

The frequency difference between the cw and ccw beam of the ring laser is directly proportional to the angular rotation rate $\Omega$. Although P and $\lambda$ do change slightly, the change induced by the Sagnac effect is insignificant and the quantity $4A/P\lambda$ is treated as a scale factor between the frequency shift, $\Delta f$, and the angular rotation rate, $\Omega$. To make a practical rotation sensor out of the ring laser, the cavity must be stabilized so that P and hence $\lambda$ do not change appreciably over time thus changing the scale factor. Normally the cavity length is stabilized to be in resonance at the center of the gain profile.

A second factor that complicates the design of laser gyros is a phenomenon called lock-in which is a coupling of the two beams to a single frequency at low angular rotation rates. Lock-in makes the laser gyro insensitive to small rotation rates and unacceptable, as such, for applications in inertial platforms. Lock-in must somehow be avoided.

Several techniques can be used to avoid the lock-in phenomenon. For instance, the cavity can be made so that one mirror dithers and only one path is in alignment at a time. Or an optical component can be added either within the cavity or outside of the cavity, to switch on and off each beam in sequence. The disadvantage of either approach is that the

frequencies are not measured at the same time and cavity noises are not correlated.

Another approach that is popularly used is to bias the gyro with a known rotation that is greater than the threshold rotation for lock-in. A pendulum type rotation, back and forth around the sensitive axis of the gyro, would integrate to zero over time and yet keep the gyro predominantly out of the lock-in region. Yet another method to avoid lock-in is to remove the gain medium from the cavity. In this scheme, the resonant cavity is passive and the laser light is transmitted into the cavity from an external source. The passive laser gyroscope will be explored more thoroughly in the next section.

Each of the techniques discussed complicates the basic design of the ring laser gyro. Inherent in each design is an additional noise component in the rotation signal, which is caused by the dither process. Currently the dither noise and the cavity finesse are the limiting factors in laser gyro accuracy. The cavity finesse is in turn limited by the quality (smoothness) of the mirrors used in the cavity; and dither noise is limited by the non-ideal performance of the added components used in the dither process.

The Passive Laser Gyroscope

A Passive Ring Laser Gyroscope (PRLG) is depicted in Fig. 10. The resonant cavity on the right is formed by the mirrors 1,2,3,and 4. A beamsplitter and two external mirrors

5 and 6, direct the light from a frequency stabilized laser
into the cw and ccw cavity modes.
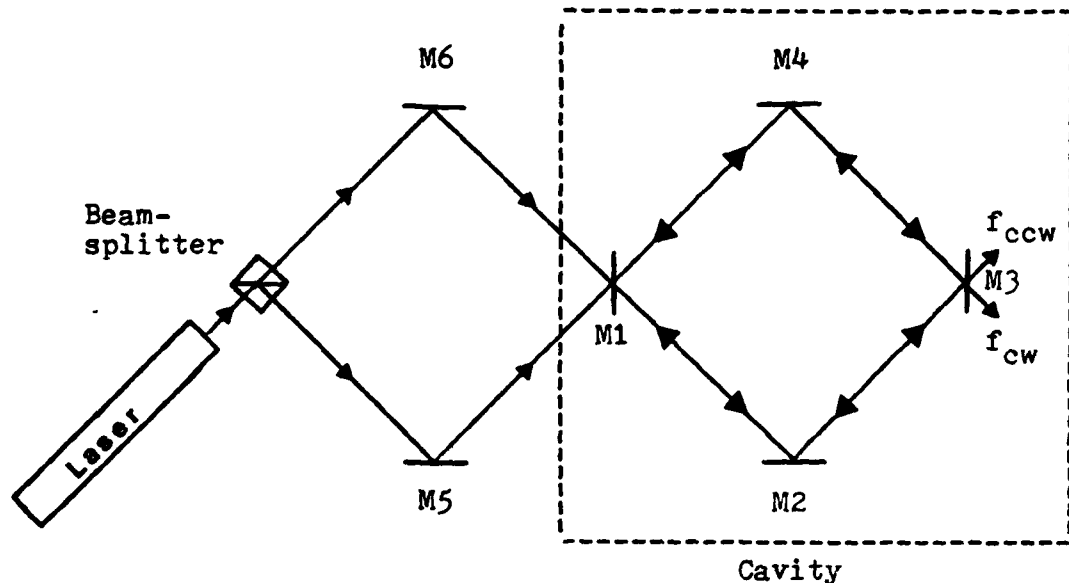


Fig. 10.  A Basic Passive Ring Laser Gyroscope

The advantage of the PRLG over the active laser gyro
is the absence of the lock-in phenomenon. The disadvantage
of the PRLG is that the laser no longer automatically lases
at the peak resonant frequency of each cavity beam. Instead,
external control loops must be added to bring each beam to
its respective resonant frequency. The control loops for the
beams are the cavity control loop, which controls the cavity
beam, and the rate control loop, which controls the rate
beam.

The cavity control loop allows the frequency of the
cavity beam to remain constant, and changes the perimeter of
the resonant cavity to bring the cavity beam into resonance.

When an angular rotation causes a shift of $\frac{1}{2}\Delta L$ in path length, the cavity loop applies a voltage to a Piezo-Electric Transducer (PZT) which in turn moves the cavity mirror until the path length has changed $-\frac{1}{2}\Delta L$, and the cavity beam is again in resonance. The PZT is a transducer whose width varies linearly with the voltage applied across it. One or two of the cavity mirrors are mounted on PZT wafers so that the cavity path can be adjusted. This is true even for active ring lasers where the cavity path length is used to frequency stabilize the laser.

The second control loop of the PRLG, the rate loop, uses an acousto-optic modulator to shift the frequency of the rate beam to keep it in resonance. The rate loop not only has to adjust for changes in resonance caused by rotation, it also has to compensate for the changes caused by the cavity loop. A constant angular rotation causes a shift in each beam path of $\frac{1}{2}\Delta L$, but the cavity control loop changes the perimeter of the cavity to counteract the Sagnac effect. The result is that the path length difference in the rate loop changes by a full $\Delta L$, half caused by the Sagnac effect, and half by the compensation of the cavity control loop. The rate control loop changes the frequency of the rate beam by $\Delta f$, Eq (19), to bring the rate loop back into resonance.

Both control loops require an error signal that indicates whether the beam is at the resonant frequency, less than the resonant frequency, or greater than the resonant frequency. The error signal for both loops is produced by

introducing a modulating signal into the cavity. The modulating signal is applied to the PZT transducer thereby changing the path length of both rate and cavity loops simultaneously. Modulating the path length is equivalent to modulating the resonant frequency, Eq (14). Figure 11 shows two cases of cavity modulation.

The first case shows the cavity being modulated about its resonant frequency. A detector monitors the power transmitted through the cavity (or reflected from the cavity). The peak power occurs when the modulating signal is zero voltage. At each minimum and maximum of the modulating signal the detector monitors a minimum power. By inputing both the modulation signal and the detector signal into a Lock-In Amplifier (LIA) a demodulated signal is produced and integrated to produce a DC error signal. Since the resonant peak is symmetrical, the demodulated signal is symmetrical about its axis. The integration of this signal yields a zero DC error signal as desired. When the modulation is not centered on the resonant peak, the demodulated signal is no longer symmetrical about its axis. The integrated value produces a DC error signal. This process is best demonstrated by considering an extreme example.

At point B in Fig. 11, the modulating signal is on the leading edge of the resonant peak. The detector senses a maximum power at the minimum of the modulating signal and conversely, senses a minimum power at the maximum of the modulating signal. When the detector signal is combined with the
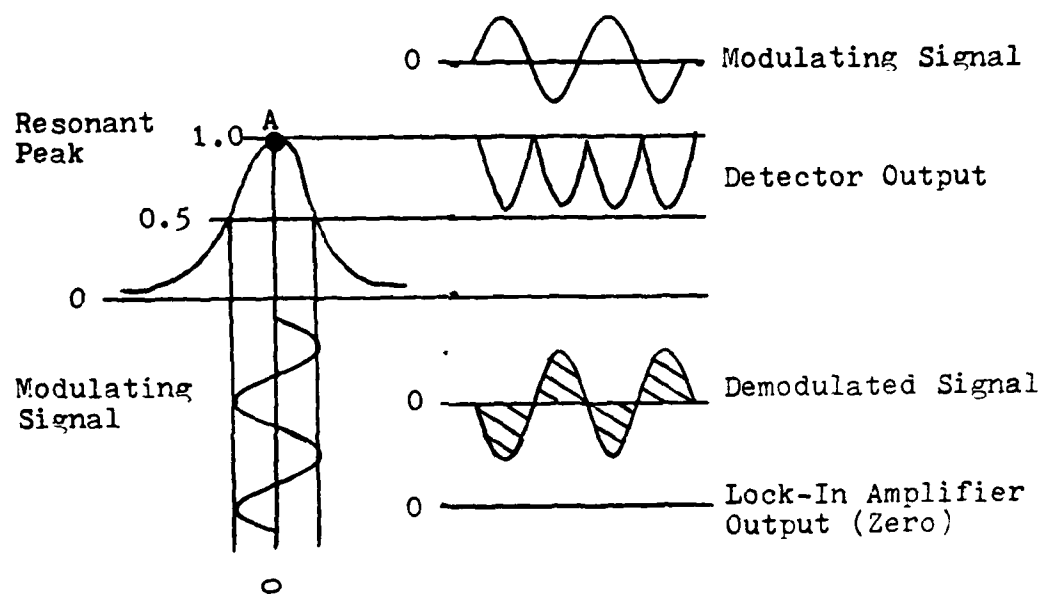
Modulation About Resonant Peak
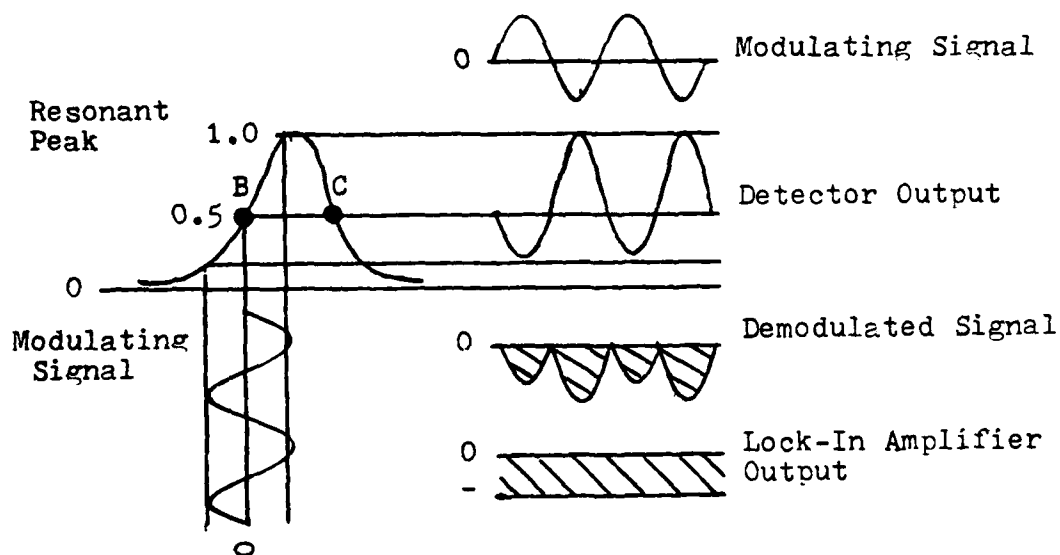


Modulation About Half Power Point

Fig. 11. Resonant Peak Detection

modulating signal in the LIA, the demodulated signal is to-
tally negative, and thus a strong DC error signal is pro-
duced. An identical but inverted detector signal and LIA out-
put is produced if the modulation is at point C.

For the control loops to be functional, the basic PRLG
shown in Fig. 10 must be modified to include a frequency
shifting transducer for the rate control loop, a PZT backed
mirror for the cavity control loop and modulation signal, and
a detector for each beam to monitor the power transmitted
(or reflected).

Even with the above modifications, there still exists a
significant problem with the simple configuration of Fig. 10,
which is the interference caused by the back reflections of
the two beams from the cavity input mirror. Not only is the
beam from mirror 5 directed into the cavity, but a portion of
the beam is reflected back from the input mirror 1 to mirror
6 and back into the laser cavity. Similarly the beam from
mirror 6 reflects off of mirror 1 and 5 back into the laser
cavity. To prevent the back reflection into the laser cavity
an isolator must be added to the beam path.

## The Acousto-optic Modulator

The acousto-otic (AO) modulator performs three functions
in the PRLG. First it shifts the frequency of the light pass-
ing through it by very precise amounts. Second it varies the
intensity of the beam. Third it acts as an isolator for each
beam path by preventing light from reflecting back into the

laser cavity.

The acousto-optic is a clever devise that shifts the frequency of light by reflecting it from a moving sound wave. The frequency change is a doppler shift caused by the moving wave. The acousto-optic operates by applying an electrical modulating signal to a shaker that converts the electrical signal to a sound wave that propagates through a glass plate. The sound wave creates areas of compression and rarefaction in the glass that have higher and lower indexes of refraction than the unstressed glass. A light beam is propagated through the glass at a grazing angle, Fig. 12, to the sound wave phase front. Each sound wave acts as a partially silvered mirror and reflects a portion of the light passing through it. If the incident angle is correct, each reflected wave will reinforce the previously reflected wave. The end result is that up to 80% of the incident light energy can be reflected by the sound waves, and since the waves are moving at 3.9 km/sec, the effect is the same as if the light were reflected from a mirror traveling at 3.9 km/sec.

The diffraction of light by sound waves is very similar to Bragg diffraction of X-rays in crystals. The angle of incidence at which the reflected light waves reinforce one another is the Bragg angle. By the nature of the geometry for Bragg diffraction, the modulating frequency of the acousto-optic is equal to the frequency shift in the reflected light. If this were only true at the Bragg angle, the acousto-optic would not be a very effective transducer in the PRLG. Fortu-
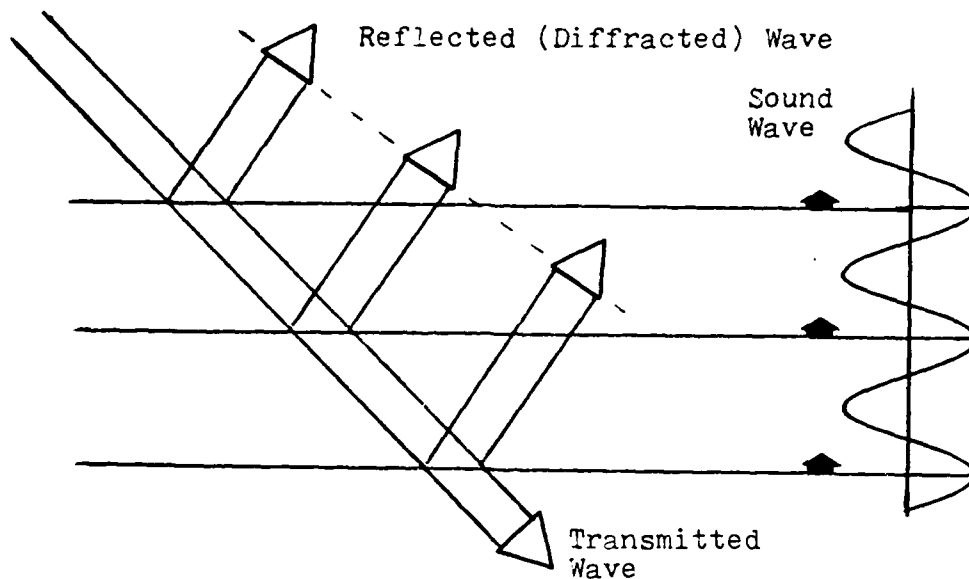
Fig. 12. Acousto-Optic Diffraction

nately this holds true at frequencies near the Bragg angle
also.

When the Bragg angle condition is not exactly met, the
reflected waves do not quite reinforce each other. The re-
sultant wave is a product of the diffraction, and is deflec-
ted from the normal angle of reflection. The frequency shift
is still equal to the acousto-optic modulation frequency, but
the direction of the diffracted wave is altered and the power
of the wave is slightly reduced. These two effects are mini-
mal for the slight frequency changes required by the PRLG.
The acousto-optic is able to adjust the frequency of the rate
beam by adjusting the modulating frequency driving the
acousto-optic.

The second function of the acousto-optic, varying the intensity of the beam, is accomplished by varying the amplitude of the modulating signal. The amplitude of the modulating signal in turn determines the force with which the shaker is driven, which determines the intensity of the sound wave propagating through the glass plate, which determines the variation in index of refraction in the sound wave, which determines the amount of light reflected at each wave, which finally determines the intensity of the diffracted beam. This effect is not linear, but it is a useful way of varying the beam intensity slightly about the desired operating point.

The third function that the acousto-optic performs in the PRLG is to isolate each forward beam path from reflecting back into the laser cavity. The acousto-optic accomplishes this because unlike reflection, the doppler frequency shift is not a reversible function. In other words, when a beam of frequency shifted light is reflected back through the acousto-optic it does not shift back to its original frequency. Instead, the beam is shifted twice in frequency and deflected so that it does not retrace the original beam path. The result is that the reflected beam is not aligned to the laser cavity and is not at the resonant frequency of the laser cavity. Because of this isolative property, an acousto-optic is added to each beam path in the PRLG.

In summary, the acousto-optic performs three functions in the PRLG simultaneously. By adjusting the modulating frequency to the acousto-optic, the rate beam is shifted to the

cavity resonant frequency. By adjusting the amplitude of the driving frequency to either acousto-optic, the beam intensities of the two beams can be equalized. This is required to minimize noise in the system. Finally, the acousto-optic modulators in each branch of the PRLG prevent a back reflection of light from destabilizing the laser cavity.

## Mode Matching

Mode matching is the final factor to be considered in designing a PRLG. In an active ring laser the resonant cavity is an integral part of the laser, and therefore there is no need to match a laser mode to a cavity mode. But in the PRLG, the laser cavity and resonant cavity are separate cavities, each with its own characteristic modes. To transfer the power from one laser mode into one resonant cavity mode, the laser mode must be shaped to coincide with the cavity mode.

If this is not done, the laser wave directed into the cavity is not stable, but changes with each round trip until the wave degenerates into one or more cavity modes. In the process, part of the energy is lost, and the rest can be distributed into more than one cavity mode. The overall effect is a loss of power transmitted through the cavity, and a decrease in effective cavity finesse.

Before the laser mode can be matched to the resonant cavity mode, one must first identify the shape and propagation characteristics of each mode. The output of the laser is a Transverse Electro-Magnetic (TEM) wave. The amplitude pro-

file of the electric field in the wave normally has one peak, as in Fig. 13a, that gradually tapers to zero at infinity in a gaussian profile ($TEM_{00}$). Unlike the sine $TEM_{00}$ mode of waveguides, Fig. 13b, the gaussian beam $TEM_{00}$ mode is not specified by its nulls, since they are at infinity. Instead another point on the profile is used where the amplitude has decreased to 0.368 (1/e) of its peak value. The radial distance from the peak amplitude at the beam center to this point is called the spot size of the beam. Eighty six percent of the beam's power is within the spot size.



a.  Gaussian $TEM_{00}$ mode     b.  Waveguide $TEM_{00}$ mode
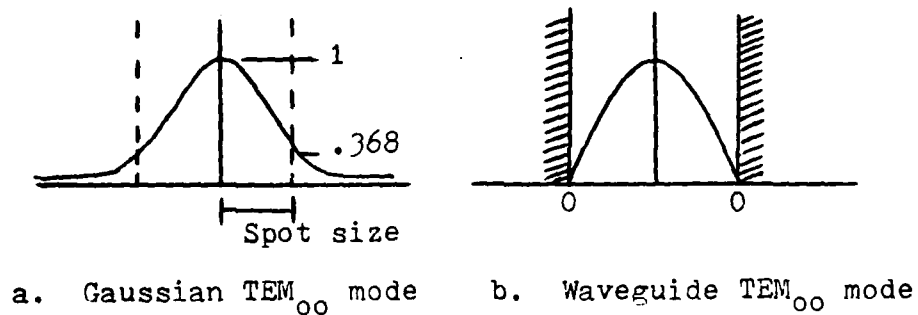
Fig. 13.  Comparison of Gaussian and Waveguide $TEM_{00}$ Modes

A second difference between the waveguide $TEM_{00}$ mode and the gaussian beam $TEM_{00}$ mode is that as the laser propagates through free space, it is not confined by the boundary conditions of the waveguide. Laser beams diffract as they propagate. Diffraction causes the energy in the beam to spread out across its phase front, Fig. 14a. The gaussian beam is unique in that the diffraction of the original gaussian wave at point A in Fig. 14a, produces another gaussian
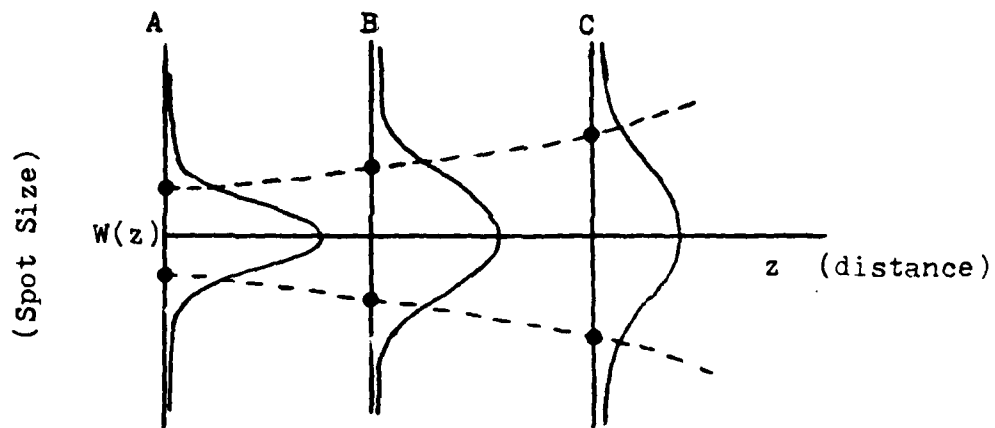
a. Three Cross Sectional Amplitude Profiles
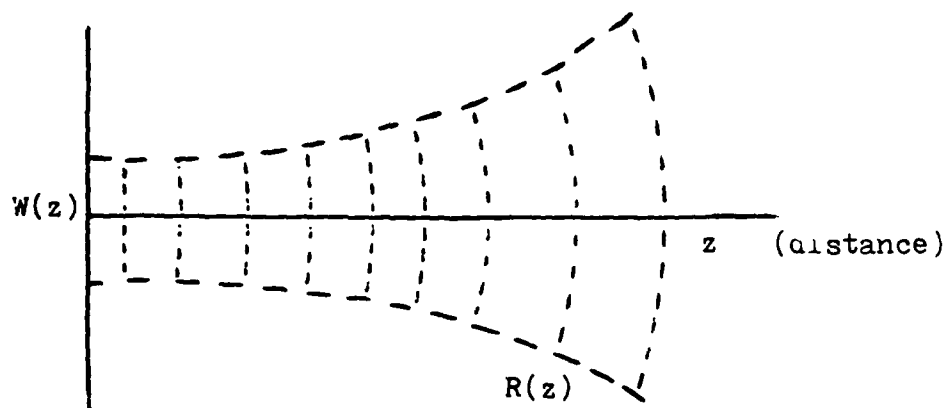


b. Isoclines of Constant Phase

Fig. 14. Propagation of a Gaussian Beam

wave at point B and point C. Diffraction produces another gaussian wave, but not an identical wave. At each progressive point, the spot size of the beam increases. The point along the beam that has the smallest spot size is defined as the waist of the beam. The spot size of the wave at any point along the laser beam can be expressed as a function of the waist spot size, the wavelength of the laser light, and the distance from the waist along the beam:

$$W(z) = W_0 \left[1 + \left(\frac{\lambda z}{\pi W_0^2}\right)\right]^{\frac{1}{2}} \qquad \text{(Ref 7:90)} \qquad (20)$$

where

$W(z)$ = beam's spot size at distance z

$z$ = distance from the waist along the beam

$W_0$ = waist spot size

$\lambda$ = wavelength of the laser light

As the laser beam propagates, the divergence of the spot size causes the phase front to curve, Fig. 14b. As the beam propagates the wave's phase front spreads out laterally. Since each point of the wave is traveling at the same speed, each point must be an equal distance from the waist. At a large distance from the waist, the radius of curvature of the beam (isocline of constant phase) equals the distance from the waist. The exact radius of curvature at any point is given by:

$$R(z) = z\left[1+\left(\frac{\pi W_o^2}{\lambda z}\right)^2\right] \qquad \text{(Ref 7:90)} \qquad (21)$$

where

$R(z)$ = radius of curvature at distance z

From Eq (21), the radius of curvature at the beam waist where z equals zero, would be infinite. So the beam is a plane wave at the waist, and a curved (spherical) wave at all other points.

A unique gaussian beam can be completely specified by its spot size and radius of curvature at any point, or by two spot sizes and the distance between them, or by two radii of curvatures and the distance between them. The characteristic gaussian $TEM_{oo}$ mode of a cavity can be found by finding the unique gaussian beam that "fits" the geometry of the cavity including the curvature of the cavity mirrors.

Consider the plano-spherical cavity of Fig. 15, consisting of a flat mirror with an infinite radius of curvature and a curved mirror with a radius of curvature $R_2$ separated by a distance L. The gaussian $TEM_{oo}$ mode must have a waist at the flat mirror, since the gaussian beam's radius of curvature is infinite only at the waist. The beam's radius of curvature at distance L, the length of the cavity, must match the radius of curvature of the second mirror. By manipulation of Eq (21) the waist of the cavity's characteristic $TEM_{oo}$ mode is:

$$W_o = \left[\frac{\lambda}{\pi}\,(LR_2)^{\frac{1}{2}}\left(1-\frac{L}{R_2}\right)^{\frac{1}{2}}\right]^{\frac{1}{2}} \qquad (22)$$

II-31
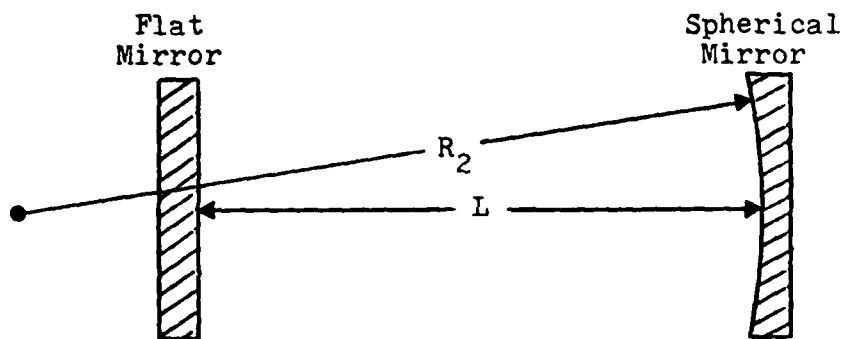
Fig. 15.   Plano-Spherical Cavity

The analysis for the plano-spherical cavity can be ex-
tended to the symmetrical square cavity of Fig. 16, consist-
ing of two opposing flat mirrors and two opposing spherical
mirrors of equal radius of curvature. A round trip through
this cavity is identical to two round trips through the
plano-spherical cavity of Fig. 15. The characteristic gauss-
ian beam "fits" the radius of curvature of each mirror. Equa-
tion (22) can be used to find the waist size of the beam. The
square cavity shown below has two waists, one at each flat
mirror.
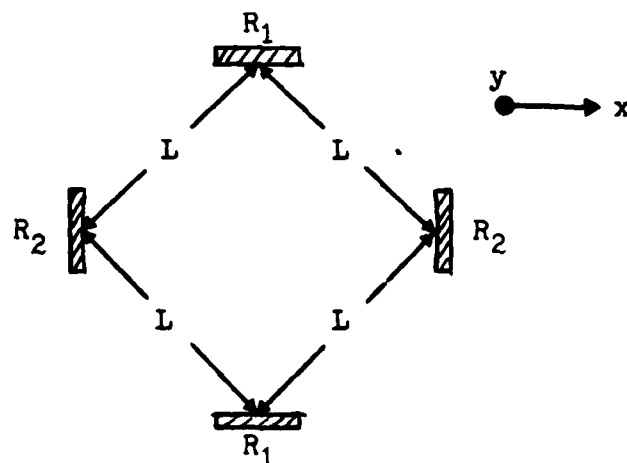


Fig. 16.   Plano-Spherical Square Cavity

There is one adjustment that must be made in equating the geometry of the square cavity to the simple plano-spherical cavity. The $45^\circ$ angle of incidence at mirror $R_2$ changes the effective radius of curvature of that mirror. Therefore the beam that "fits" $R_2$ is different in the square cavity from the beam that "fits" $R_2$ in the simple cavity, even though the length L is identical.
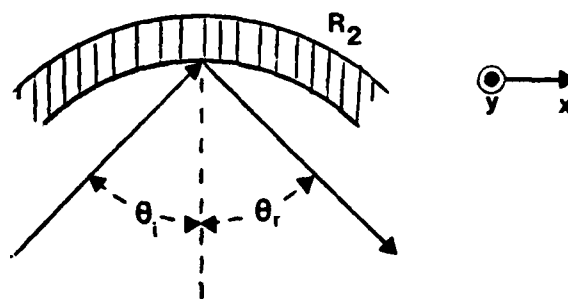


Fig. 17. Astigmatism of a Spherical Mirror in a Ring Cavity

For the curved mirror, $R_2$, of the square cavity, light is incident at a $45^\circ$ angle. The effective radius of curvature in the horizontal or x-axis (in the plane of incidence) is;

$$R_{2x} = R_2 \cos\theta \qquad (\text{Ref } 7:42) \qquad (23)$$

where

$R_{2x}$ = effective radius of curvature of $R_2$ in the
    x-axis

$R_2$ = true radius of curvature

$\theta$ = angle of incidence (from normal)

Similarly, the effective radius of curvature in the vertical

or y-axis (perpendicular to the plane of incidence) is;

$$R_{2y} = \frac{R_2}{\cos\theta} \qquad \text{(Ref 7:42)} \qquad (24)$$

where

$R_{2y}$ = effective radius of curvature of $R_2$ in the
y-axis

The spherical mirror $R_2$, due to astigmatic effects, acts as
an elliptical mirror in the square cavity. It has a different
effective radius of curvature in each plane x and y, namely
radii of $R_{2x}$ and $R_{2y}$ given by Eqs (23) and (24). The gaussian
beam that "fits" the square cavity is found independently in
the x and y plane. Since radii of curvatures $R_{2x}$ and $R_{2y}$ are
different, the waists found in the x and y planes must be
different also. In other words, the gaussian beam that "fits"
the cavity is elliptical.

Once the mode of the laser and the mode of the cavity
are identified by a waist size and location, the entire beam
of each can be determined using Eqs (20) and (21). Identify-
ing the modes is the first step in any mode matching techni-
que. Four cases are now presented.

The simplest mode match is possible when matching a cir-
cular $TEM_{00}$ laser mode to a circular $TEM_{00}$ cavity mode. A
circular mode, as opposed to an elliptical mode, refers to a
beam which has the same spot size in the lateral x and y
axes. Figure 18 shows the laser and cavity placed a fixed
distance apart. Equation (20) is used to project the spot

sizes of each beam as they propagate toward each other. The beams are sketched in Fig. 18. A point C can be found where the spot sizes of the two beams are identical. The radius of curvature of each beam can be found at point C by using the appropriate distance z in Eq (21). By inserting a lens at point C it is possible to convert the radius of curvature of the laser beam to the radius of curvature of the cavity beam. The laser beam is "focused" into the cavity. The focal length of the lens must be;

$$F = \frac{R_C R_L}{R_C - R_L} \qquad (25)$$

where

    $F$ = focal length of the lens

    $R_L$ = radius of curvature of laser beam at point C

    $R_C$ = radius of curvature of cavity beam at point C
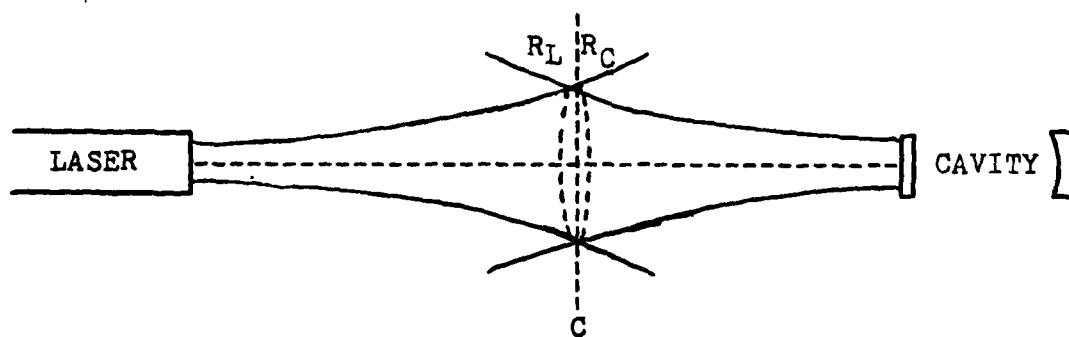


Fig. 18.  Case I: Circular-Circular Mode Match

The characteristic mode of the laser has been matched to the
characteristic mode of the cavity. This example of a mode
match demonstrates how a lens can be used to change the ra-
dius of curvature of the beam at a given spot size, and thus,
transform it into another unique gaussian beam. This same
principle is applied in case II to eliminate the restriction
of having to place the lens at one fixed point as in the
previous example.
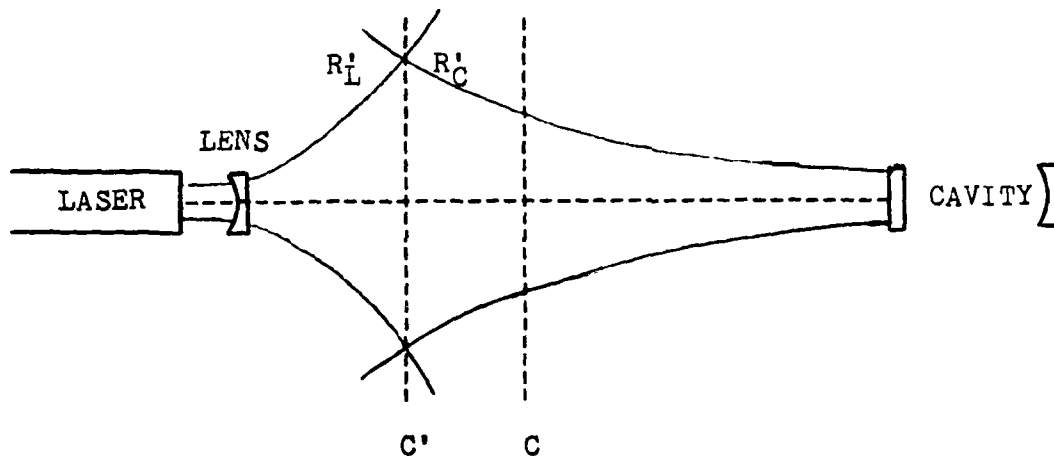


Fig. 19.   Case II:  Circular-Circular Mode Match Using a
           Diverging Lens

By inserting a diverging lens near the laser, as shown in
Fig. 19, the point at which the spot sizes are identical can
be shifted from point C to point C'.

When the circular mode of the laser must match the el-
liptical mode of the square cavity, the mode matching becomes
more complex. The simplest, but not the most economical, meth-
od is to match each axis separately using the first method.
Figure 20 displays the top and side view of the laser and

cavity beams. The laser and y-axis cavity spot sizes match at point $C_y$. The laser and horizontal cavity spot sizes match at point $C_x$. By inserting a cylindrical lens at each point $C_y$ and $C_x$, the radius of curvature of each axis of the laser beam can be matched to the cavity beam's radius of curvature independently. A cylindrical lens, whose focusing surface is a section of a cylinder, has the property of focusing in only one axis of the beam and passing the other axis unchanged.
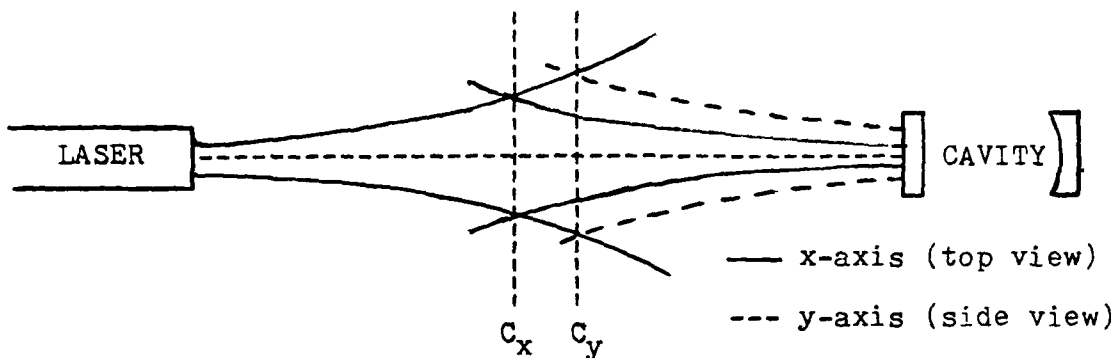


Fig. 20.  Circular-Elliptical Mode Match

It is also possible to mode match the laser to the elliptical mode of the square cavity by using two spherical lenses. This technique uses astigmatic focusing, the same effect that produced the elliptical cavity mode. The same relationships hold true for the curved surface of a lens as well as a mirror. Since the focal length of a lens is proportional to the radius of curvature of the lens' surface, Eqs (23) and (24) can be rewritten in terms of focal length:

$$F_x = F \cos\theta \qquad\qquad (26)$$

II-37

and

$$F_y = F / \cos\theta \qquad\qquad (27)$$

where

$F$ = true focal length of the lens

$\theta$ = angle of incidence (Fig. 17)

$F_x$ = effective focal length in x-axis

$F_y$ = effective focal length in y-axis

The mode matching is accomplished by first placing a diverging lens in front of the laser as in Fig. 21. The lens is rotated until the diverging x-axis beam and the diverging y-axis beam match their corresponding cavity beams at the same point C. Figure 21 shows the vertical beam of the laser diverging more rapidly due to astigmatism to meet the wider axis of the cavity's elliptical mode. The effective focal length of the diverging lens is shorter in the y-axis than in the x-axis.
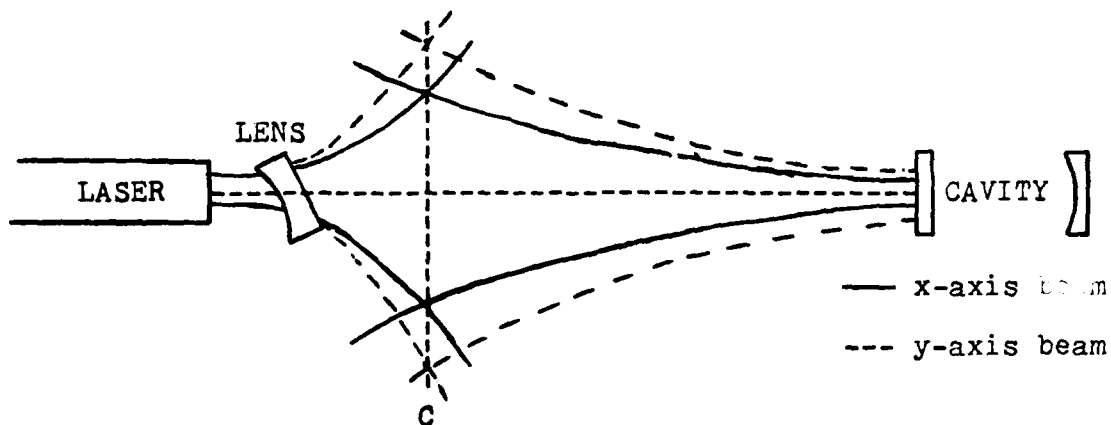


Fig. 21. Elliptical-Elliptical Mode Matching Using a Diverging Lens

Once the spot sizes are matched at the same point, the
next step can be accomplished. There are four radii of cur-
vatures that must be matched by the lens placed at point C.
The radius of curvature of the y-axis laser beam at point C,
$R_{Ly}$, is matched to the radius of curvature of the y-axis of
the cavity beam at point C, $R_{Cy}$, by a lens with the focal
length, $F_y$, given by;

$$F_y = \frac{R_{Cy} \cdot R_{Ly}}{R_{Cy} - R_{Ly}} \tag{28}$$

And similarly, the radius of curvature of the x-axis laser
beam at point C, $R_{Lx}$, is matched to the radius of curvature
of the x-axis of the cavity beam at point C, $R_{Cx}$, by a lens
with the focal length, $F_x$, given by;

$$F_x = \frac{R_{Cx} \cdot R_{Lx}}{R_{Cx} - R_{Lx}} \tag{29}$$

The mode match could be made by placing an elliptical
lens at point C with focal lengths of $F_x$ and $F_y$. The match
can also be made using a spherical lens of some focal length
$F_?$ rotated at some angle $\theta$, such that;

$$F_? = F_y \cdot \cos\theta \tag{30}$$

and,

$$F_? = F_x / \cos\theta \tag{31}$$

By substituting $F_x / \cos\theta$ into Eq (30) for $F_?$ and solving
for $\theta$;

$$\theta = \cos^{-1} (F_x / F_y)^{\frac{1}{2}} \tag{32}$$

Then, substituting this result back into Eq (30) and solving for $F_?$:

$$F_? = (F_x \cdot F_y)^{\frac{1}{2}} \tag{33}$$

Thus the laser mode is matched to the elliptical mode of the cavity by two spherical lenses. The advantage of this method is the economy of using available spherical lenses rather than special ordering cylindrical or elliptical lenses. The primary disadvantage is the difficulty of properly placing the lenses.

# III. CONFIGURATION DESIGNS

Now that the theory behind PRLG's has been presented in Chapter II, the two configurations introduced in Chapter I are discussed in more detail. The first configuration is depicted in Fig. 22. The second configuration is depicted in Fig. 23.

The primary difference between the two configurations is the method in which resonance is detected. In the first configuration, Fig. 22, light is transmitted through the cavity and detected as it exits. The detector signal voltage varies in amplitude as the cavity is scanned to produce the resonant peak shown in Fig. 22. The second configuration, Fig. 23, detects the light reflected from the input mirrors. When the cavity is in resonance, light is transmitted through the cavity and thus less light is reflected from the input mirror. The detector signal voltage varies in amplitude as the cavity is scanned to produce the resonant valley shown in Fig. 23.

A second difference between the two configurations is the method in which the laser beam is mode matched to the resonant cavity. In the first configuration, a simple mode match is accomplished by placing spherical mirrors to focus the beam at a point where the spot size of the laser beam equals the geometric mean of the cavity spot sizes in the x and y axes. The spherical mirror focuses the radius of curvature of the laser to match the geometric mean of the cavity's radii of curvatures in the x and y axes.

DETECTOR

PZT

DETECTOR

MIRROR

ACOUSTO-
OPTIC

PZT

PELLICLE

MIRROR

ACOUSTO-
OPTIC

LASER

POLARIZING
BEAM-SPLITTER

(Detector Voltage)

(Scan Voltage)

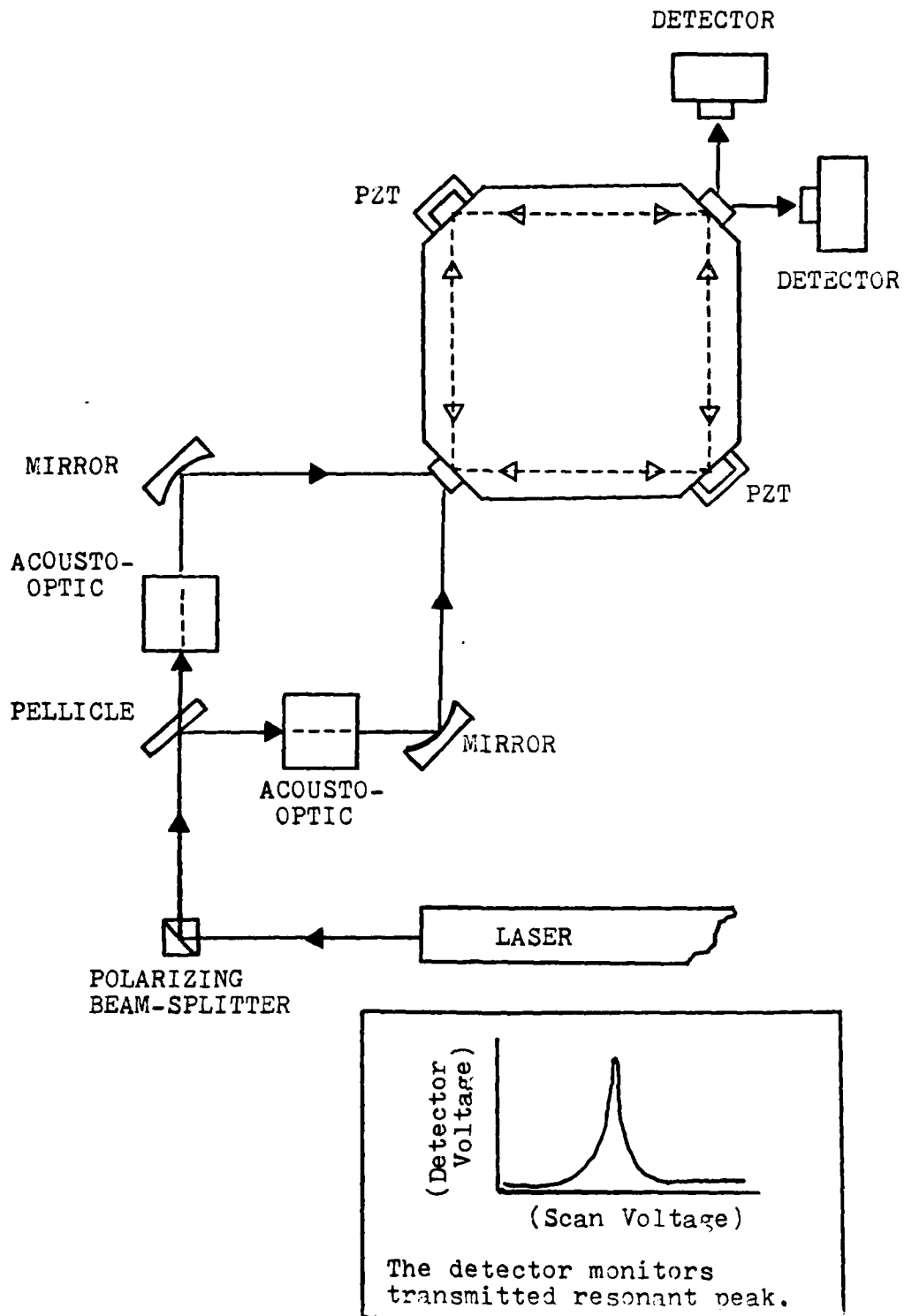The detector monitors
transmitted resonant peak.
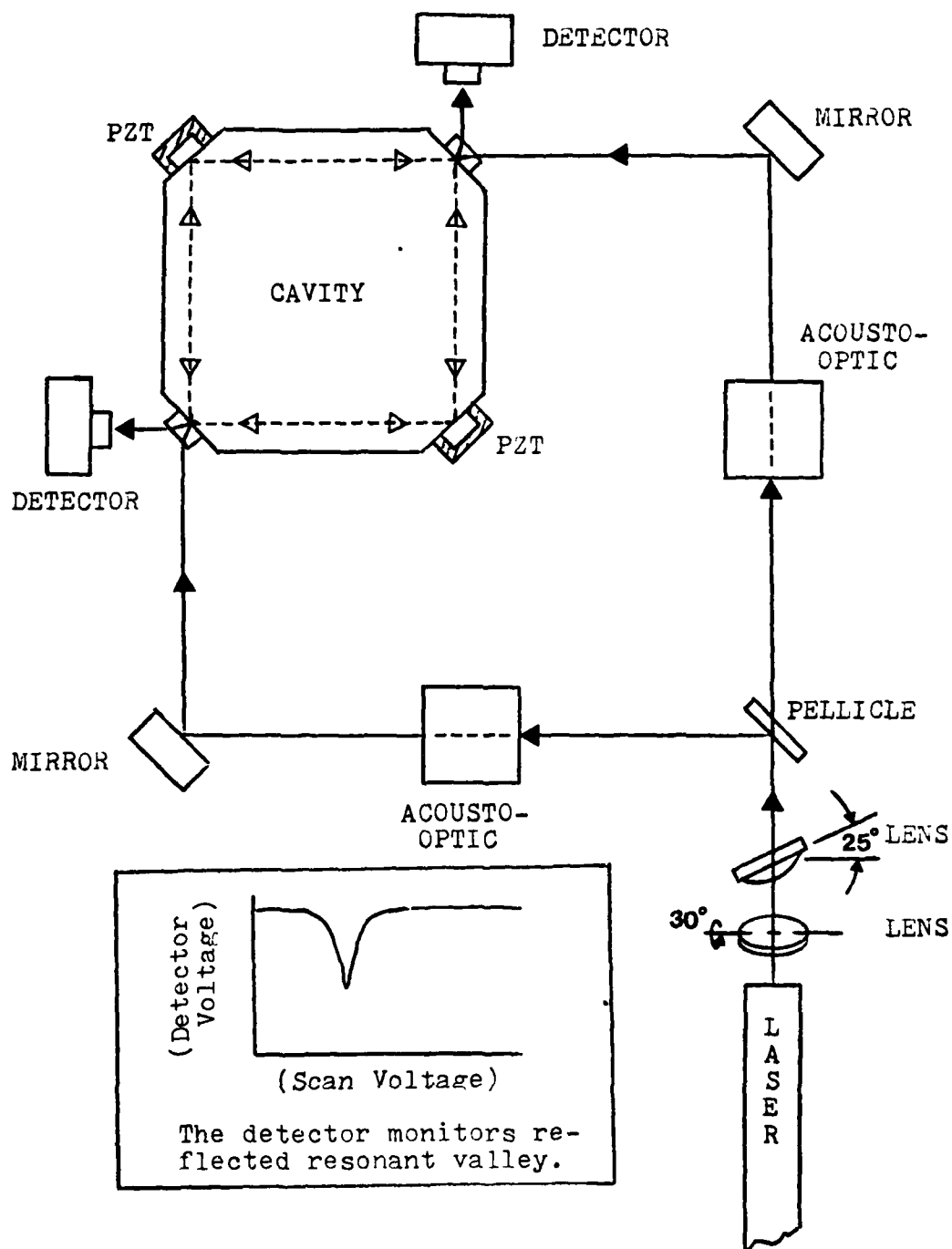
Fig. 22.   First Configuration of the PRLG

Fig. 23. Second Configuration of the PRLG

The second configuration mode matches using the last technique of Chapter II. The astigmatism of a diverging lens is used to match the laser spot size to both the x and y axes cavity spot sizes. Astigmatism in a converging lens is used to match the two laser radii of curvatures to the two cavity radii of curvatures. Another version of the second configuration which uses cylindrical lenses to mode match the beams is designed and built, but not tested due to an equipment failure. It is presented in Appendix A for future reference.

The other components used in each design are either identical or equivalent components. The same resonant cavity is used in both configurations. The acousto-optic modulators are different models but have identical performance characteristics. The same frequency stabilized laser is used, and although the pellicles used are different they are equivalent. The detectors are the same, and the associated electrical control circuits between the detectors, acousto-optics, and PZT transducers are identical with minor adjustments.

The major component of both configurations is the optical resonant cavity provided by Rockwell International. It is the high finesse of this cavity that enables both configurations to measure low rotation rates. The cavity is a square symmetrical cavity of 9.525 cm on each side, Fig. 24. Mirrors 1 and 2 are flat and serve as either input or output mirrors. Mirrors 3 and 4 are curved with a radius of curvature of 800 cm. Both mirrors are backed by a PZT push on with a 0-300 volt dynamic range. All mirrors are mounted on a solid Zero-

MIRROR 2
R=∞
(input/
output)

MIRROR 4
R= 800 cm

PZT

PZT

MIRROR 3
R= 800 cm

MIRROR 1
R=∞
(input/output)

|← 9.525 cm →|
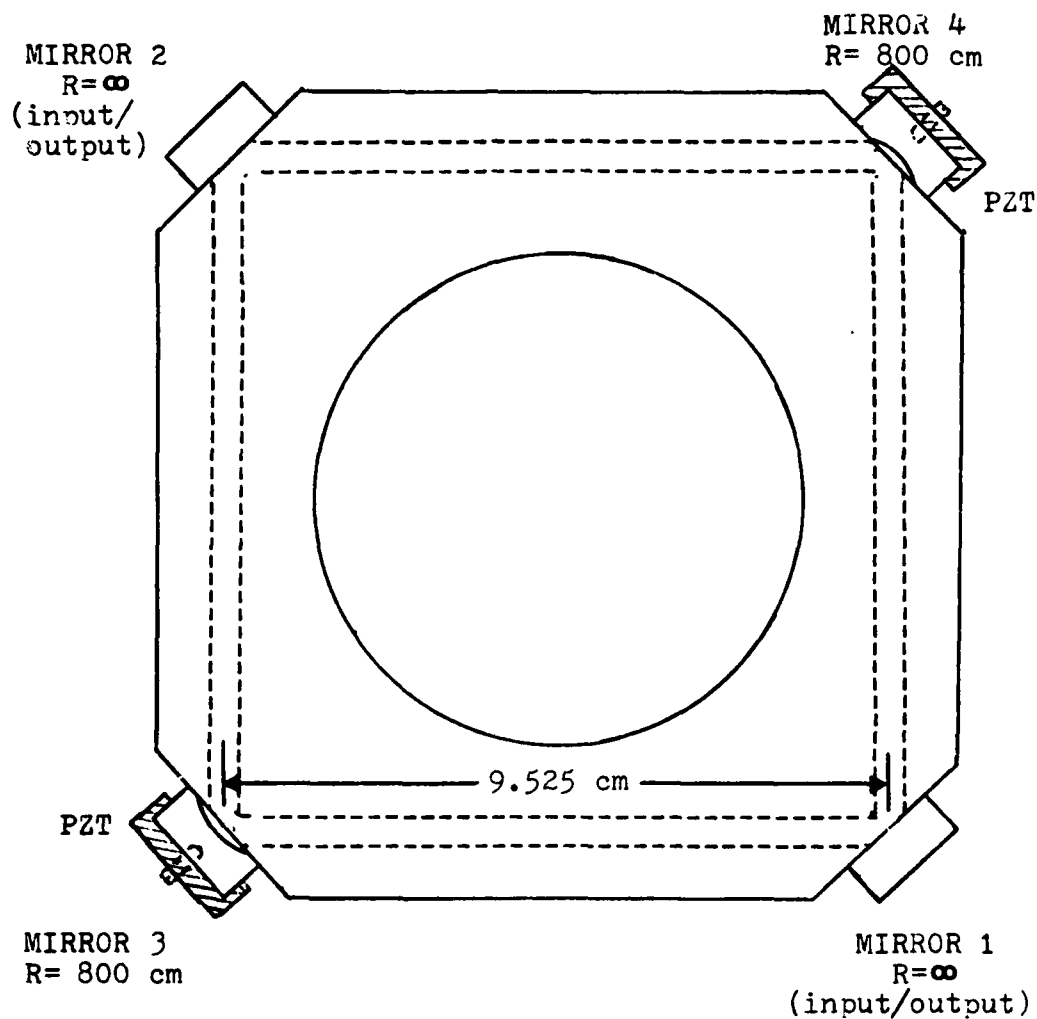
Fig. 24. Rockwell International Resonant Cavity

dur block with paths drilled for the cavity beam. The cavity
is evacuated and partially back-filled with a mixture of
Helium and Neon gas. The cavity mirrors consist of 23 dielec-
tric layers on a Zerodur substrate (Ref 1). The reflectivity
of each mirror is 0.99995 (Ref 1). The smoothness of the mir-
ror surfaces is approximately 0.5 $\overset{o}{A}$ $_{rms}$ or $\lambda/12656$ $_{rms}$ ex-
pressed in wavelengths (Ref 1). The theoretical finesse of

the cavity considering only the reflectivity of the cavity mirrors is given by Eq (15) with $R_1R_2R_3R_4$ substituted for $R_1R_2R_3$:

$$\frac{n(0.99995)}{1-(0.99995)^2} = 31,415 \qquad (34)$$

The actual finesse of the cavity was estimated by Rockwell International to be 10,000 or one-third the theoretical finesse of an ideal cavity with the same reflectivity. The degradation of finesse is largely due to the phase distortion caused by the mirror surface as discussed in Chapter II. The maximum finesse the spatial phase distortion allows is 12,656.

The characteristic $TEM_{00}$ mode of the cavity can be determined using the plano-spherical cavity equation, Eq (20), and the effective radii of curvatures of the cavity mirrors, Eqs (21) and (22). The effective radii of curvatures for the flat mirrors are infinite in both the horizontal and vertical plane. The effective radii of curvatures for the 800 cm mirrors are 1131 cm in the vertical plane and 566 cm in the horizontal plane. From Eq (20), the waist size of the cavity beam at both flat mirrors is an ellipse with a semi-axis of 0.0456 cm vertically and 0.0383 cm horizontally as shown in Fig. 25.
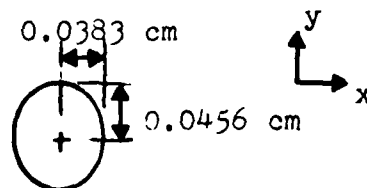


Fig. 25. Waist of the Cavity $TEM_{00}$ Mode

The scale factor relating angular rotation and the frequency difference in the cavity beams can be determined using Eq (19):

$$\Delta f = \frac{4A}{P\lambda} \Omega \qquad (19)$$

By substituting $L^2$ for A and 4L for P the scale factor of $4A/P$ in Eq (19) reduces to $L/\lambda$;

$$\Delta f = \frac{9.525 \text{ cm}}{6.323 \times 10^{-5}} \Omega = 1.5 \times 10^5 \Omega \qquad (19')$$

This scale factor linearly transforms the rotation rate of the cavity in radians per second into the frequency difference in hertz between the cw and ccw cavity beams. To relate the frequency difference to angular velocity expressed in earthrate, $\omega_{ie}$, the scale factor must be adjusted. Earthrate is the angular velocity of the earth in the equatorial plane or $15.041°/\text{hr}$. This equates to $7.2921 \times 10^{-5}$ rad/sec. Multiplying by $7.2921 \times 10^{-5}$, the scale factor of Eq (19') becomes 10.976. A rotation of one earthrate will produce a shift of 10.976 Hz between the cw and ccw cavity beams.

The theoretical transmission of the cavity in resonance is determined from Eq (15) with $R_2 R_3 R_4$ substituted for $R_2 R_3$:

$$T = \frac{(1-R_1)(1-R_2 R_3 R_4)}{\left[1 - (R_1 R_2 R_3 R_4)^{\frac{1}{2}}\right]^2} \qquad (35)$$

Since $R_1 = R_2 = R_3 = R_4 = 0.99995$, Eq (35) yields:

$$T = \frac{(1-0.99995)(1-0.99995^3)}{\left[1 - (0.99995)^2\right]^2} = 0.75 \qquad (36)$$

The power transmitted through the cavity is equally transmitted through mirrors 2, 3, and 4, so the power transmitted through any one output mirror is 25%. The reflectance from the input mirror must equal the difference between incident power and transmitted power. So the reflected power at resonance is also 25% of the incident power. When the cavity is not in resonance the input mirror acts as a simple mirror. Essentially no power is transmitted and 99.995% of the incident beam is reflected.

The above values of reflectance and transmission do not account for absorbtion, scattering, and the phase distortion of the cavity beam. These effects reduce the transmittance of the cavity in resonance. The spatial distortion of the phase front increases the reflectance at resonance.

# IV.  DATA

The data taken for each configuration falls into two general categories, alignment data and performance data. The alignment data includes measurements of beam intensity, FSR, $\Delta f_{\frac{1}{2}}$, and finesse. In the second configuration, an additional measurement is made to test mode matching. The performance data includes first a calibration measurement used to identify a scale factor between the rate-loop error voltage and the angular rotation rate of the cavity. Next the noise level in the error signal is measured. These two measurements are used to determine the rotation sensitivity of the PRLG. In the second configuration, a measurement of long term bias drift in the error signal is compared to the difference in intensity of the two beam paths.

Beam intensity measurements are taken at three locations for each beam. The first measurement compares the intensity of each beam as it leaves the beam splitter. The second compares intensities leaving the acousto-optics. The third compares the cavity transmission for each beam. These measurements are taken during the initial alignment of the PRLG, and are not indicative of intensities during operation. Before final alignment the beam intensities leaving the acousto-optics are equalized.

The FSR, $\Delta f_{\frac{1}{2}}$, and finesse are experimentally determined by applying a saw-tooth scan voltage to the PZT's of the cavity. The difference in scan voltage between two adjacent resonant peaks is proportional to the FSR. The difference in

scan voltage between resonant peak half-power points is pro-
portional to the $\Delta f_{\frac{1}{2}}$. Since finesse is a unitless measure, it
can be found by dividing the scan voltage proportional to the
FSR by the scan voltage proportional to $\Delta f_{\frac{1}{2}}$. It is assumed
that the cavity perimeter is a linear function of the PZT
voltage. This assumption is valid as long as the PZT's are
properly preloaded. Preloading applies a constant force be-
tween the PZT and the cavity mirror so that a change in PZT
width moves the cavity mirror an equivalent distance. A
change in the preload force that the PZT's apply to the cav-
ity mirrors can change the FSR proportional voltage and the
$\Delta f_{\frac{1}{2}}$ proportional voltage. Thus both measurements must be made
with the same PZT preload force.

Alignment data was not available for the first series of
measurements which were taken in the first configuration.
Other alignment data is contained in Tables I and II. Figure
26 traces the resonant profile of the PRLG in the first con-
figuration as a scan voltage is applied. The voltage at each
resonant peak is recorded to determine the proportional FSR
voltage. The FSR proportional voltage in Fig. 26 is 54.4
volts. Figure 27 displays the expanded resonant peak of the
first configuration which is used to determine the proportion-
al $\Delta f_{\frac{1}{2}}$ voltage. The faint line sweeping the bottom half of
figure is the scan voltage. The upper peak is the cw beam's
resonant peak. The lower peak is the ccw beam's resonant peak.
There are 1.5 divisions between the resonant peak half-power
points. The scan voltage changes 4mV/Div. Then $\Delta f_{\frac{1}{2}}$'s

proportional voltage is 6mV, and the finesse is:

$$F = \frac{54.4 \text{ volts}}{0.006 \text{ volts}} = 9067$$

These values appear in the first row of Table II.

## TABLE I

### Alignment Data: Beam Intensities

| Configuration | Trial | Beam Direction | Beam Splitter Output | Acousto-Optic Output | Cavity Transmission | Cavity Reflection |
|---|---|---|---|---|---|---|
| 1 | 2 | cw | 236 µw | 195 µw | 3.7 µw | ------- |
| 1 | 2 | ccw | 274 µw | 200 µw | 1.7 µw | ------- |
| 2 | 1 | cw | 130 µw | 90 µw | 1.7 µw | 78-88 µw |
| 2 | 1 | ccw | 224 µw | 153 µw | 2.7 µw | 112-129µw |

## TABLE II

### Alignment Data: Finesse Measurements

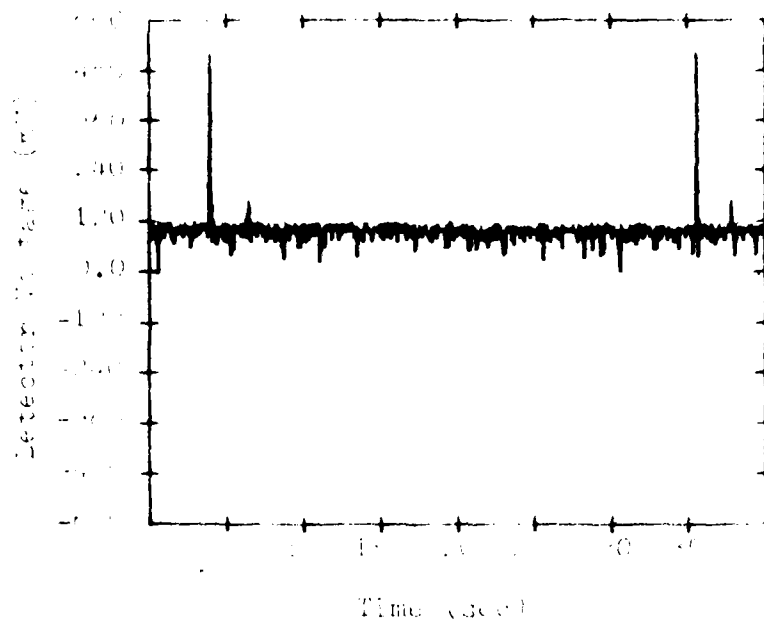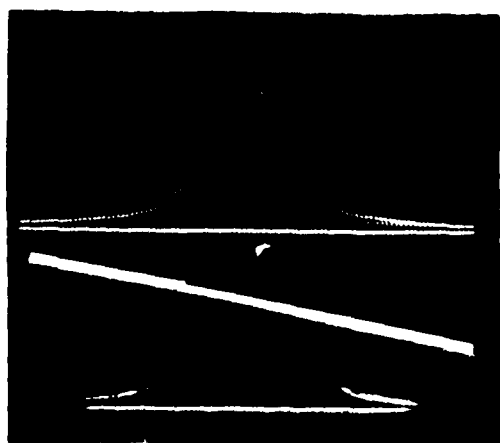| Configuration | Trial | Scan Voltage FSR | Scan Voltage $\Delta f_{\frac{1}{2}}$ | Finesse |
|---|---|---|---|---|
| 1 | 2 | 54.4 volts | 0.006 volts | 9067 |
| 2 | 1 | 51.7 volts | 0.0111 volts | 4658 |
| 2 | 2 | 51.7 volts | 0.0067 volts | 7716 |

Fig. 26. Onolog Free Spectral Range



Scan Voltage    50mV/Div

Detector
Voltage 1 x 2   20mV/Di

Time Scan    0.02m V/Di

Fig. 27.   Resonant Peaks: First Fundamental Pair, Second Pair

Figure 28 depicts the resonant profile of the PRLG in
the second configuration as the scan voltage is applied.
The scan voltage is the decreasing ramp. The lower peak is
the resonant peak of the beam transmitted through the cavity.
The upper valley is the profile of the beam reflected from
the cavity input mirror. The $\Delta f_{\frac{1}{2}}$ proportional voltage of the
peak is identical to the $\Delta f_{\frac{1}{2}}$ proportional voltage of the val-
ley. Once both beams are aligned, the resonant valley of each
beam is used to determine the finesse of the PRLG. Figure 29
depicts the inverted resonant valley and the scan voltage
used to determine the $\Delta f_{\frac{1}{2}}$ proportional voltage and hence the
cavity finesse for the last data series. The 1.2 divisions
between half-power points correspond to 6.7 mV of scan vol-
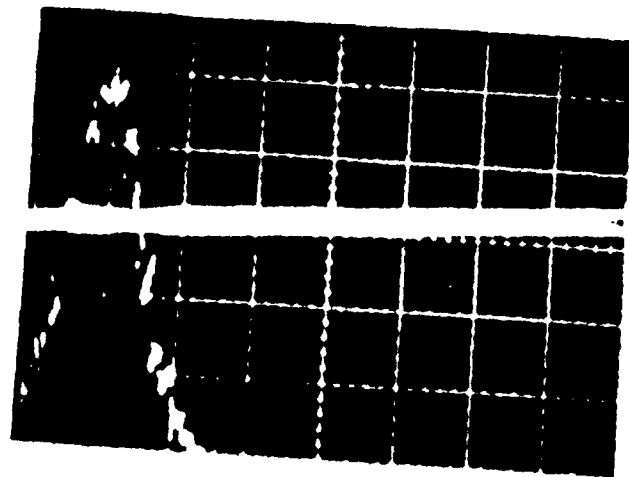tage. The resultant finesse is 7716.
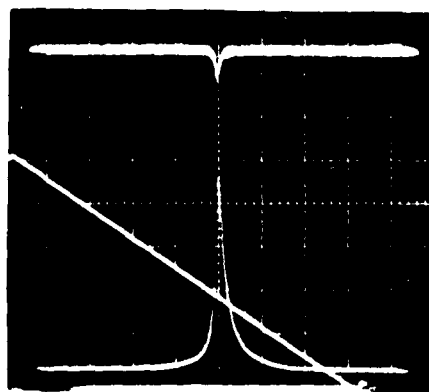


Scan Voltage   100mV/Div

Detector
Voltage of     20mV/Div
Transmission

Detector
Voltage of     50mV/Div
Reflectance

Fig. 28.   Resonant Peak/ Valley: Second Configuration, First
Trial

Scan Voltage    100mV/Div

Fig. 29.    Inverted Resonant Valley: Second Configuration,
Second Trial

An additional comparative measurement is made in the
second configuration to confirm that the laser mode and the
cavity mode are matched. This is done by comparing the reso-
nant valley of the total reflected beam to the resonant val-
ley of an apertured beam. Consider the case where the modes
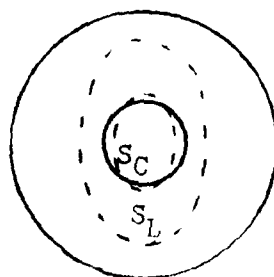are not matched, as in Fig. 30.



Fig. 30.    Laser and Cavity Modes

The incident beam of the laser forms spot $S_L$ which is
larger than the spot of the cavity mode, $S_C$. When the

IV-6

reflected beam is unapertured, the detector collects essen-
tially the total power of both beams. The detector is repre-
sented by the outer circle of Fig. 30. When the reflected
beam is apertured, more of the power of the cavity mode
passes through the aperture than of the laser mode. The aper-
ture is represented by the inner solid circle of Fig. 30. As
a result of the depicted mismatch, the resonant valley of the
apertured beam will be deeper than the resonant valley of the
unapertured beam. On the other hand, if the modes are matched,
then $S_C$ and $S_L$ are identical. The resonant valleys are also
identical for both beams.

The mode match measurement is taken using the ccw beam
of the PRLG. The depth of the resonant valley for the unaper-
tured reflected beam is $(129\mu w - 112\mu w)/129\mu w = 13\%$. When the
reflected beam is apertured as in Fig. 30, the relative depth
of the resonant valley increases to 21%, indicating the laser
mode spot is larger than the cavity mode spot. The beams are
not properly matched. This data measurement tests only for
the correct spot size at the input mirror. It does not indi-
cate whether the curvature of the beam is flat or not at the
input mirror.

The rotation sensitivity of the PRLG for each configura-
tion is determined by a series of measurements. During the
test the PRLG is not rotated. Instead, the rotation is simu-
lated by changing the beam frequency of the cw beam. Using
the scale factor from Chapter III, an angular rotation of one
earthrate, $\omega_{ie}$, can be simulated by a frequency shift of

10.976 Hz between the cavity beams. By shifting the frequency
of the cw beam by a known amount, and then measuring the re-
sultant shift in the error signal voltage (output of the rate
loop LIA) a new scale factor is determined. The new scale
factor relates angular rotation to error voltage. Consider
the first trial of configuration one, Fig. 31. The frequency
is shifted from 40 MHz plus 190 Hz to 40MHz plus 210 Hz. The
error signal changes 3.3 divisions or 66mV. The scale factor
is found by:

$$66mV/20Hz \times 10.976Hz/\omega_{ie} = 36.221mV/\omega_{ie} \qquad (37)$$

The new scale factor equates 36.221 mV of the error signal
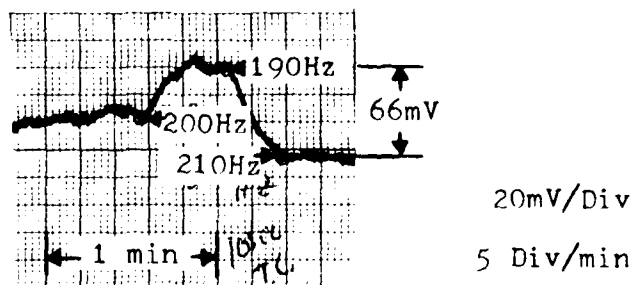voltage to an angular rotation rate of one earthrate.



Fig. 31.   Calibration for First Trial First Configuration

Next, while the frequency of the cw beam is held con-
stant, the error signal noise is measured. For the first
error signal measurement, Fig. 32, the integration time con-
stant of the LIA is set to one second. The peak to peak de-
viation in the error signal is assumed to correspond to six
standard deviations, $\sigma$, of the signal noise. Since 99.1% of

all gaussian noise falls within 3 $\sigma$'s of the mean, but only 99% falls within 2 $\sigma$'s of the mean, the peak to peak noise over the measured interval more closely approximates 6 $\sigma$'s. In Fig. 32, the peak to peak voltage spans 1.8 divisions or 90 mV. One sixth of this value or 15 mV corresponds to the measured standard deviation of the noise. By converting the noise voltage into a rotation rate by the use of the new scale factor, a Noise Equivalent Rotation (NER) rate is computed equalling 0.415 $\omega_{ie}$. At the NER rate the noise in the signal is equal to the signal strength.
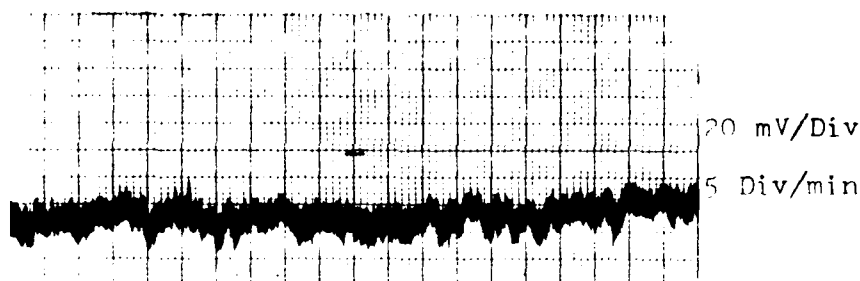


20 mV/Div

5 Div/min

Fig. 32.   Error Signal: First Configuration, First Trial, One
Second Integration, First Data Point

A second measurement, Fig. 33, yeilds 0.461 $\omega_{ie}$, a value within 10% of the first measurement. The process is repeated for LIA integration times of ten seconds and one hundred seconds. The output of the LIA is integrated to produce a DC error signal from the modulation signal. But in addition, the integration acts as a low pass filter. An increase in integration time limits the bandwidth of the noise passed through the control loop. Two data measurements are made for each

integration time. Figures 34,35,36, and 37 display the error
signals for ten second and one hundred second integration
times respectively. The results are summarized in Table III.
Major Gerry Shaw and 2Lt. Frank Rand of the F.J. Seiler
Research Laboratory recorded the first data set.



50 mV/Div

5 Div/min

Fig. 33. Error Signal: First Configuration, First Trial, One
Second Integration, Second Data Point
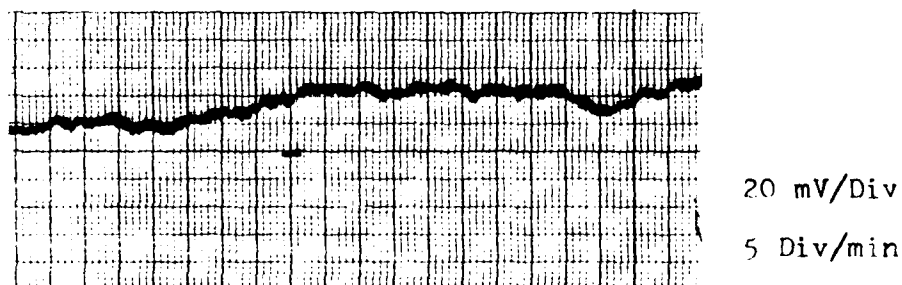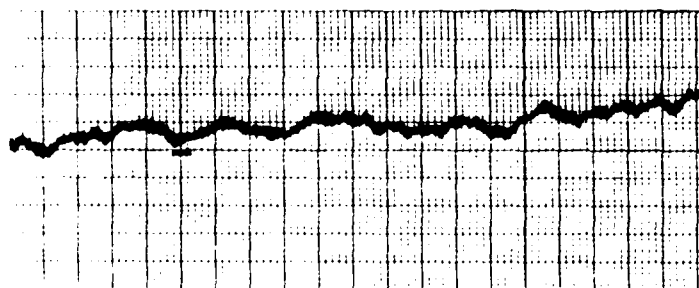


20 mV/Div

5 Div/min

Fig. 34. Error Signal: First Configuration, First Trial, Ten
Second Integration, First Data Point
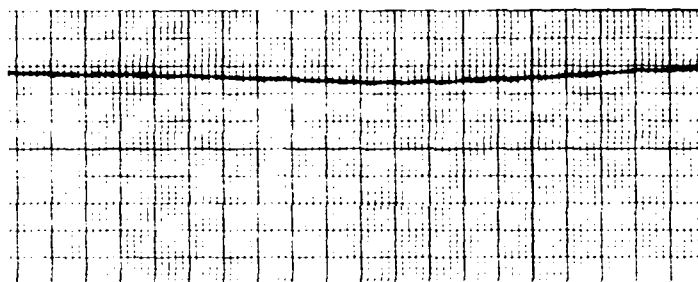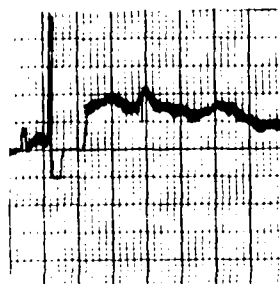
20 mV/Div

5 Div/min

Fig. 35. Error Signal: First Configuration, First Trial, Ten
Second Integration, Second Data Point



20 mV/Div

5 Div/min

Fig. 36. Error Signal: First Configuration, First Trial, One
Hundred Second Integration, First Data Point



5 mV/Div

5 Div/min

Fig. 37. Error Signal: First Configuration, First Trial, One
Hundred Second Integration, Second Data Point

## TABLE III

### Error Signal Noise: First Configuration First Trial

| Integration Time | Peak to Peak Voltage | $6\sigma\ (\omega_{ie})$ | $\sigma\ (\omega_{ie})$ |
|---|---|---|---|
| 1 sec | 1.8 Div = 90 mV | 2.49 | 0.415 |
| 1 sec | 2.0 Div = 100 mV | 2.76 | 0.461 |
| 10 sec | 0.4 Div = 8 mV | 0.22 | 0.037 |
| 10 sec | 0.4 Div = 8 mV | 0.22 | 0.037 |
| 100 sec | 0.18 Div = 3.6 mV | 0.100 | 0.017 |
| 100 sec | 0.5 Div = 2.5 mV | 0.069 | 0.012 |

The second data set is again taken in the first config-
uration. The scale factor is determined from the calibration
measurement of Fig. 38. The frequency shifts 10 Hz, while the
error signal changes from -122 mV to 251 mV, a change of
373 mV. The scale factor for this series is;

$$373\text{mV}/100\text{Hz} \times 10.976\text{Hz}/\omega_{ie} = 409.4\text{mV}/\omega_{ie} \qquad (38)$$

The error signals for one second, ten second, and one hundred
second integration times are shown in Figs. 39, 40, and 41
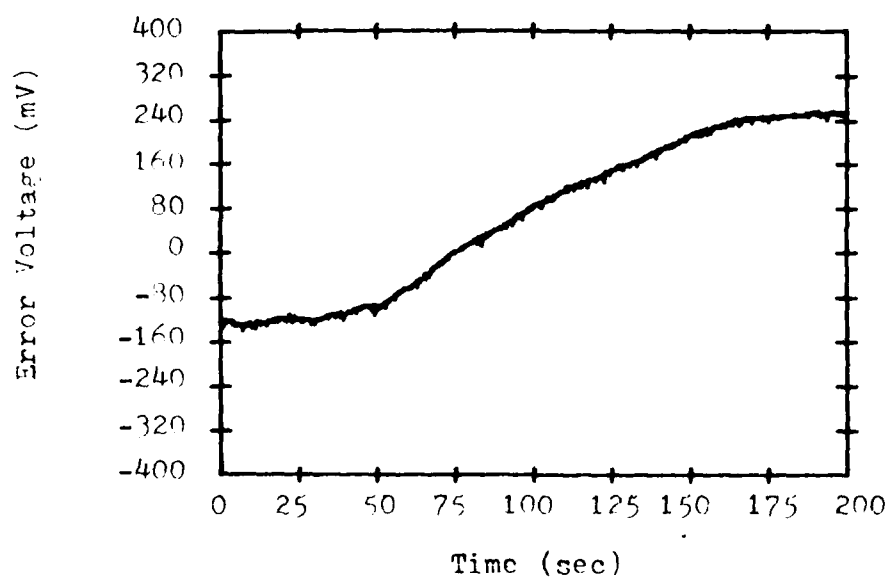respectively. The results are tabulated in Table IV.

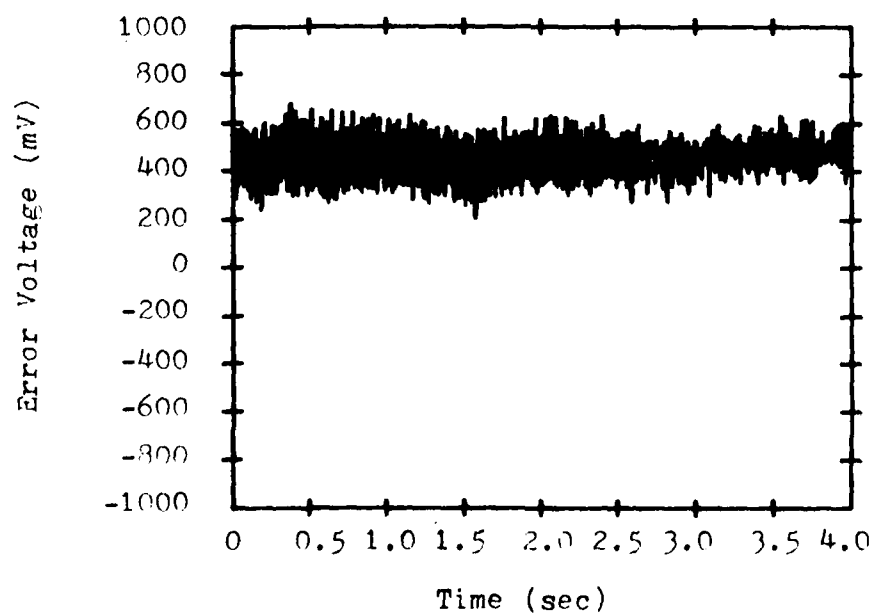Fig. 38. Calibration for Second Trial First Configuration



Fig. 39. Error Signal: First Configuration, Second Trial,
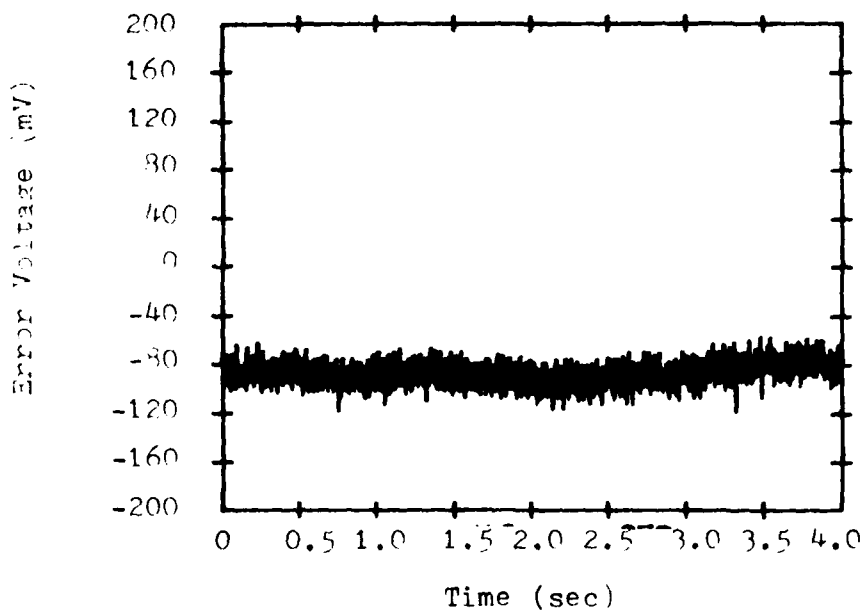One Second Integration

IV-13

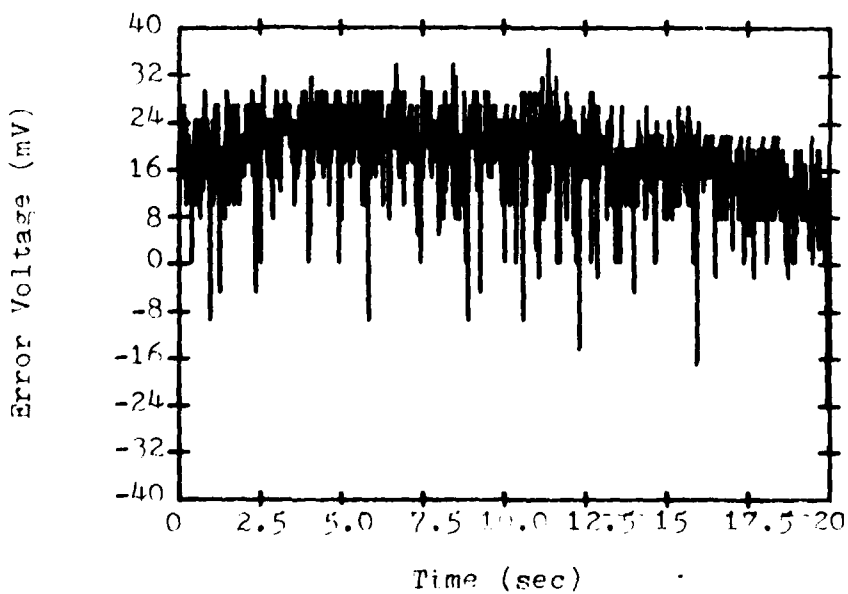Fig. 40. Error Signal: First Configuration, Second Trial,
Ten Second Integration



Fig. 41. Error Signal: First Configuration, Second Trial,
One Hundred Second Integration

IV-14

## TABLE IV

### Error Signal Noise: First Configuration Second Trial

| Integration Time | Peak to Peak Voltage | $6\sigma$ $(\omega_{ie})$ | $\sigma$ $(\omega_{ie})$ |
|---|---|---|---|
| 1 sec | 432 mV | 1.06 | 0.176 |
| 10 sec | 63.6 mV | 0.156 | 0.026 |
| 100 sec | 42.9 mV | 0.105 | 0.018 |

Two sets of data are also recorded in the second configuration of the PRLG. For the first data set, the PRLG is aligned to a finesse of 4658. The scale factor is determined from 29 frequency shifts of 100 Hz. A sample of the calibration signal for seven shifts is shown in Fig. 42. The mean voltage shift in response to the 29 frequency shifts is 2.620 volts with a mean standard deviation of 0.011 volts. The use of multiple readings decreases the effect of bias drift in the determination of a scale factor. The scale factor for this series is:

$$2620 \text{mV}/100 \text{Hz} \times 10.976 \text{Hz}/\omega_{ie} = 286.8 \text{ mV}/\omega_{ie} \qquad (39)$$

The error signals for one second, ten second, and one hundred second integration times are displayed in Figs. 43, 44, and 45 respectively. The results are tabulated in Table V.
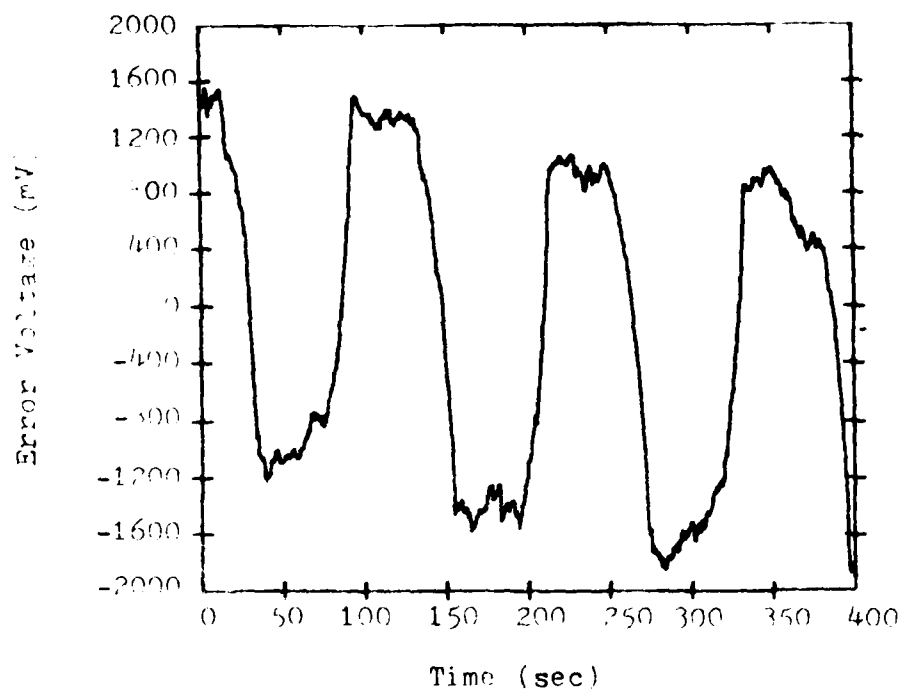
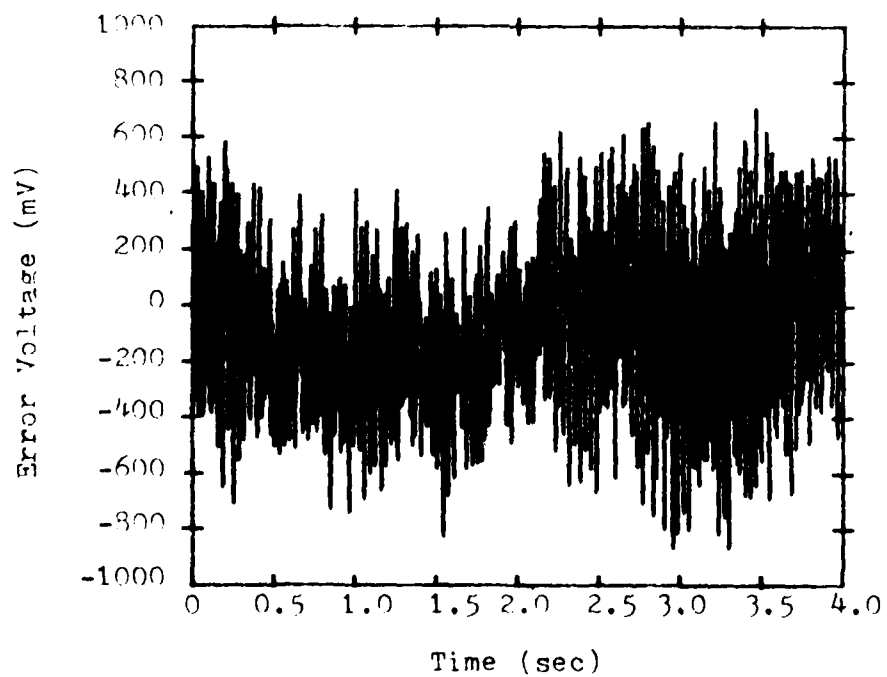Fig. 42. Calibration for First Trial Second Configuration



Fig. 43. Error Signal: Second Configuration, First Trial, One Second Integration

Fig. 44. Error Signal: Second Configuration, First Trial, Ten Second Integration



Fig. 45. Error Signal: Second Configuration, First Trial, One Hundred Second Integration

IV-17

### TABLE V

Error Signal Noise: Second Configuration First Trial

| Integration Time | Peak to Peak Voltage | $6\sigma(\omega_{ie})$ | $\sigma(\omega_{ie})$ |
|---|---|---|---|
| 1 sec | 1588 mV | 5.537 | 0.923 |
| 10 sec | 122.5 mV | 0.427 | 0.071 |
| 100 sec | 60.0 mV | 0.209 | 0.035 |

The last data set is taken after the PRLG is realigned to a finesse of 7716. Both the intensity and the finesse of the cw and ccw cavity beams are equalized prior to data sampling. The sensitivity of the LIA preamplifier is maximized. The scale factor is determined from 31 frequency shifts of 44 Hz. A sample of 7 shifts is shown in Fig. 46. The mean voltage shift in response to the 31 frequency shifts is 7.118 volts with a mean standard deviation of 0.036 volts. The scale factor for this series is;

$$7118mV/44Hz \times 10.976Hz/\omega_{ie} = 1770.8mV/\omega_{ie} \qquad (40)$$

The error signals for one second, ten second, and one hundred second integration times are displayed in Figs. 47, 48, and 49 respectively. The results are tabulated in Table VI.
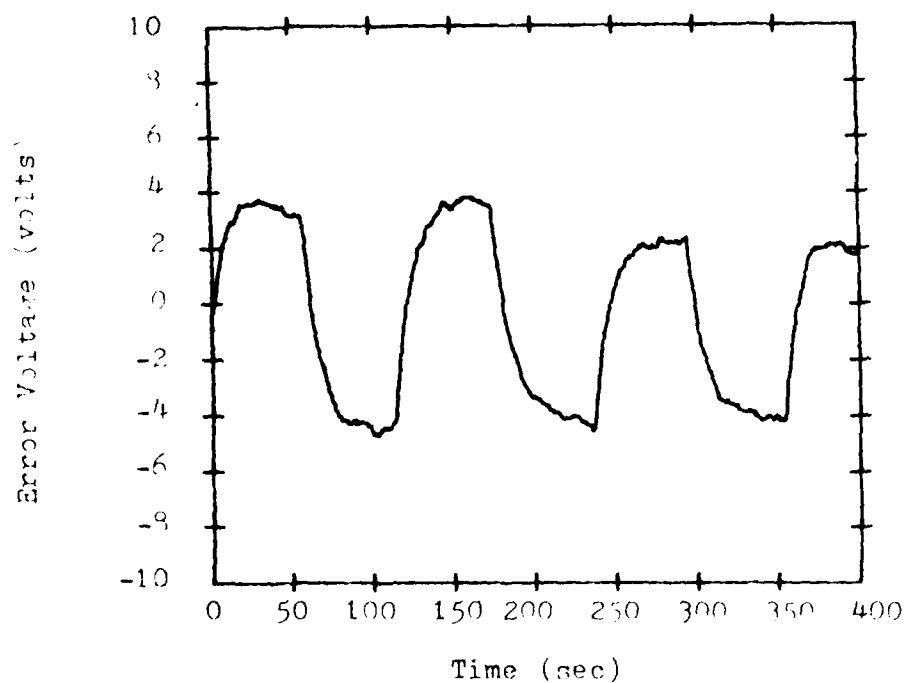
Fig. 46. Calibration for Second Trial Second Configuration
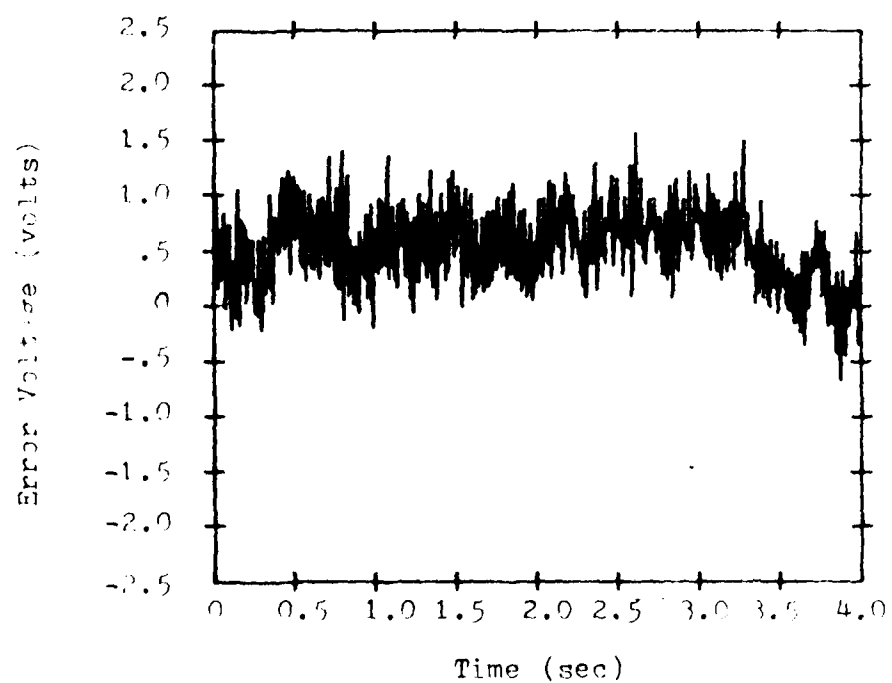


Fig. 47. Error Signal: Second Configuration, Second Trial, One Second Integration
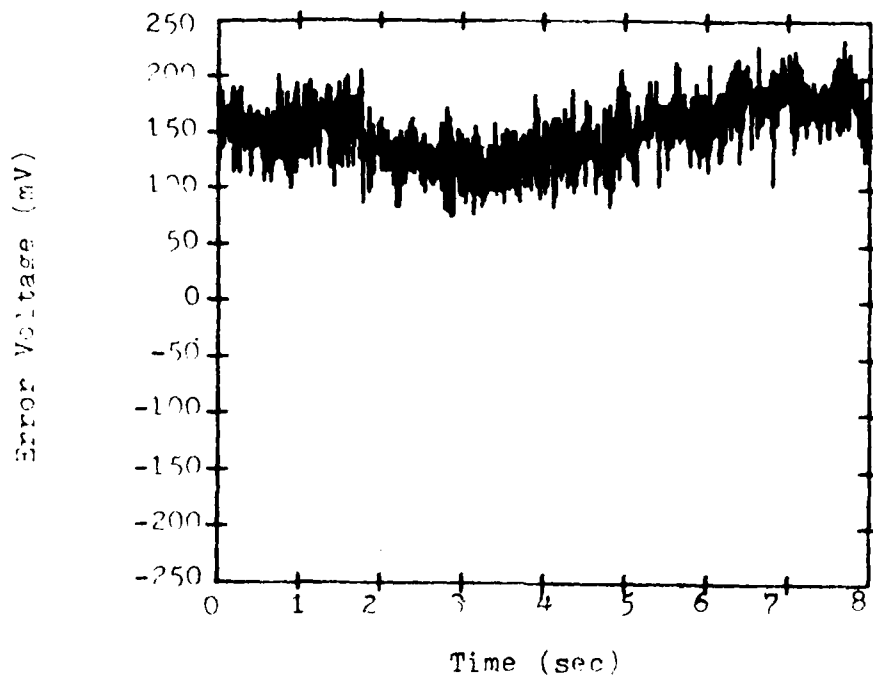
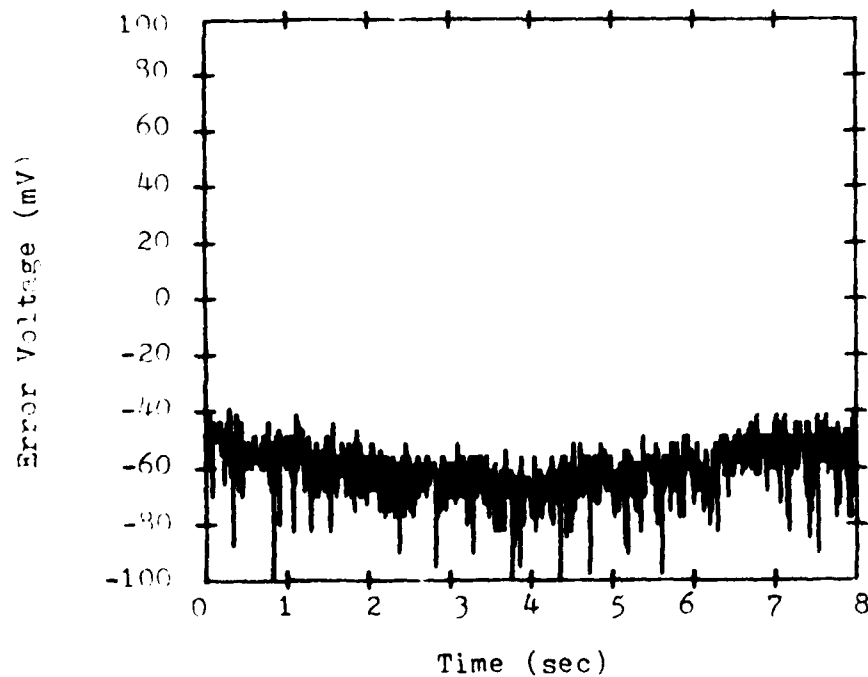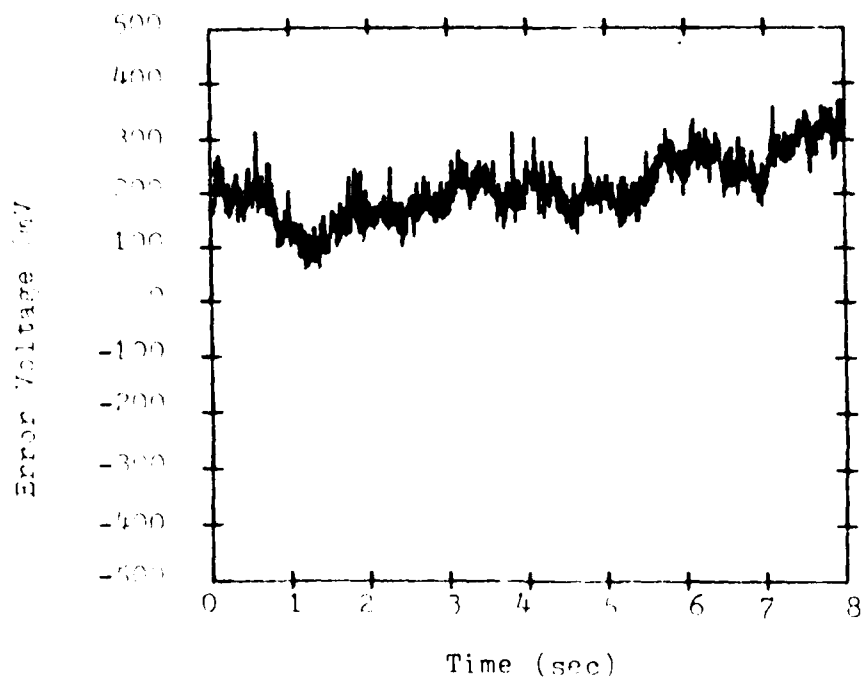Fig. 48. Error Signal: Second Configuration, Second Trial, Ten Second Integration
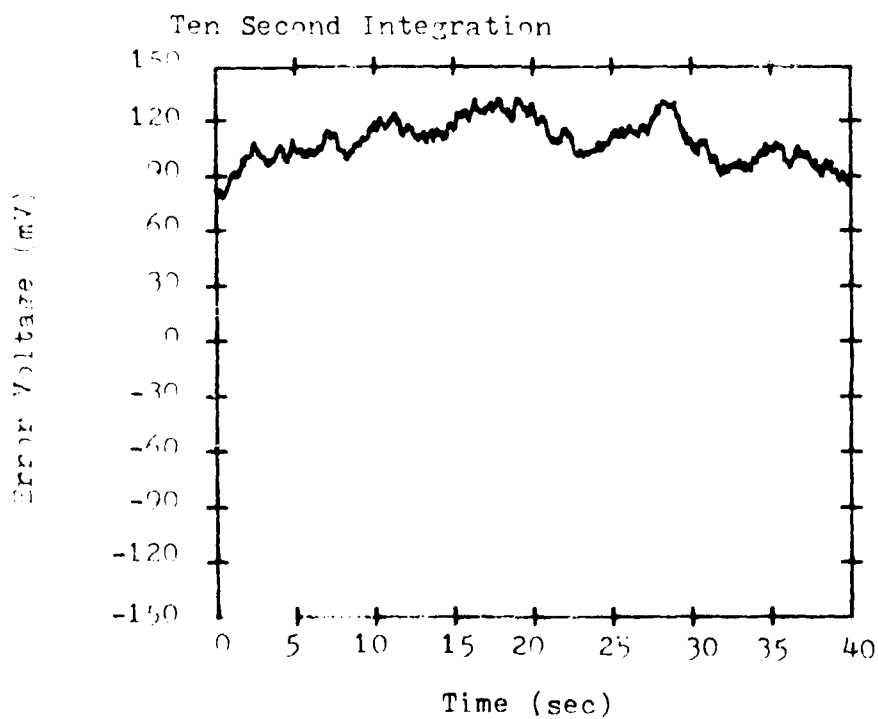


Fig. 49. Error Signal: Second Configuration, Second Trial, One Hundred Second Integration

IV-20

## TABLE VI

### Error Signal Noise: Second Configuration Second Trial

| Integration Time | Peak to Peak Voltage | | $6\sigma\ (\omega_{ie})$ | $\sigma\ (\omega_{ie})$ |
|---|---|---|---|---|
| 1 sec | 1600 | mV | 0.904 | 0.151 |
| 10 sec | 190 | mV | 0.107 | 0.01⁵ |
| 100 sec | 42 | mV | 0.0237 | 0.004 |

Finally, a bias drift measurement is recorded to corre-
late the drift in the error signal voltage to changes in the
beam intensity of the cw and ccw beams. Figure 50 displays
the error signal voltage with a plot of the difference in
beam intensities directly below. Additionally the intensity
of each beam is recorded. The scale factor for the error sig-
nal is approximately $330mV/\omega_{ie}$ or $1.6\ Div/\omega_{ie}$. The error sig-
nal varies approximately one earthrate over the 30 minute in-
terval, while the difference in beam intensities changes in
zero to approximately 2.8 mV.
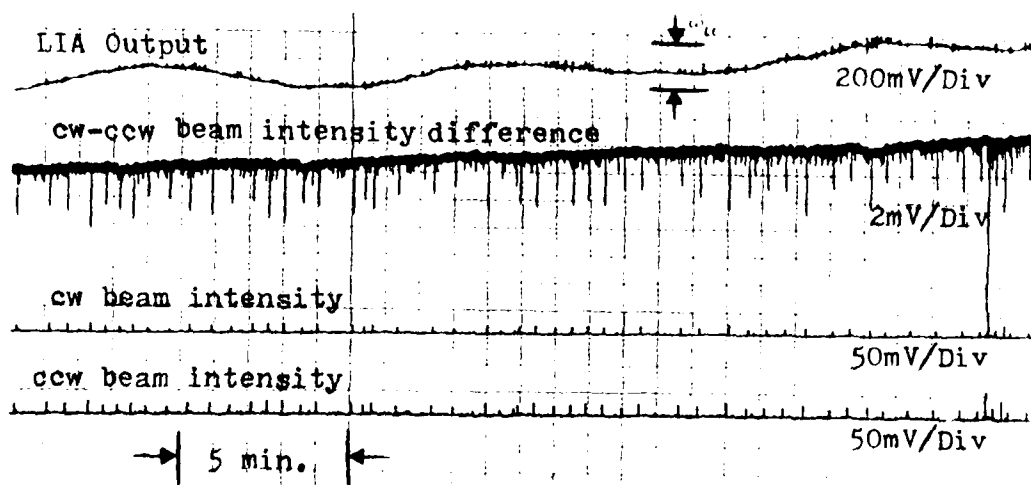


Fig. 50. Bias Drift Versus Beam Intensities

Now that each configuration has been thoroughly tested, and the Noise Equivalent Rotation (NER) rate computed in each case, the two configurations can be compared. To ease this comparison, the NER's for each trial are repeated in Table VII.

TABLE VII

Comparison of Error Signal Noise in Four Trials

| Trial | Configuration | 1 sec $\sigma$ | 10 sec $\sigma$ | 100 sec $\sigma$ | Finesse |
|-------|---------------|----------------|-----------------|------------------|---------|
| 1 | 1 | 0.461 | 0.037 | 0.012 | ---- |
| 2 | 1 | 0.176 | 0.026 | 0.018 | 9067 |
| 1 | 2 | 0.923 | 0.071 | 0.035 | 4658 |
| 2 | 2 | 0.151 | 0.018 | 0.004 | 7716 |

## V. ANALYSIS, CONCLUSIONS, AND RECOMMENDATIONS

### Analysis

Although the theoretical transmittance through each cavity mirror was computed to be 25%, the actual values, as expected, were much less. Table I shows a 3.7 μw beam as the strongest signal transmitted through the cavity. The transmittance of this signal would be 3.7 μw/195 μw or 0.019. Even allowing for the 10.1% reflection loss at the air-glass interface of the input and output mirror, the transmittance of the strongest signal is only 2.3%.

A similar result was obtained for the reflectance. The reflected beam decreases from 129 μw to 112 μw. This corresponds to a decrease in reflectance from 99.995% to 86.8%. No adjustment is made for the air-glass reflection loss since both maximum and minimum powers are identically attenuated. The theoretical value for minimum reflectance in a lossless cavity is 25%, as figured in Chapter III.

Part of the degradation in transmittance is due to imperfect alignment of the cavity. In neither case was the finesse measured at the rated finesse of the cavity. Part of the degradation is due to the spatial distortion of the resonant cavity wave by the imperfect mirror surfaces. This effect has already been discussed in Chapter II. Finally, a portion of the degradation in transmittance is due to the mode mismatch. As demonstrated by the data, a reflectance minimum of 79% can be obtained by simply aperturing the reflected beam. If the beams are properly mode-matched, the

minimum reflectance could be well below 79%. Note that the aperturing of the beam compares only the spot size match. Additional energy is lost when the radii of curvatures of the laser and cavity modes are not matched. Maximizing cavity transmittance would improve PRLG performance by increasing the detector signal strength, thus reducing the effects of shot noise and thermal noise in the signal. A more sensitive factor is the finesse of the cavity. There is a drastic change in sensitivity for configuration two as the finesse increases from 4657 to 7716.

A comparison of the two configurations proves the second to be superior to the first. Although the measured finesse in the first configuration was greater, the second trial of the second configuration produced superior results. There are two obvious advantages in using the reflected beam for the detector signal. First, the resonant valley in the reflected beam is larger than the resonant peak of the transmitted beam. From Table II, the measured resonant valley is almost six times as great as the resonant peak. The theoretical calculations predicted that the resonant valley would be three times as great. The second obvious advantage is that the beam intensity of the cw and ccw paths can be measured directly from the detector signal. This is not possible using the transmitted beam since both finesse and the incident beam intensity determine the amplitude of the resonant peak. By using the reflected beam, it is possible to both equalize beam intensities and cavity finesse for the two beam paths

prior to measuring rotation sensitivity. This procedure sig-
nificantly reduces the noise in the error signal and enables
the second configuration to triple the sensitivity of the
first configuration, and to near the goal of one milli-
earthrate sensitivity. The major drawback of using the re-
flected beam is the difficulty of preliminary alignment. It
is less difficult to detect some light being transmitted
through the cavity, than it is to detect slightly less light
being reflected from the cavity input mirror. Preliminary
alignment in this configuration is accomplished by blocking
one beam and observing the transmission of the other. Then
the aligned beam is blocked and the transmission of the
other beam is observed. This prodedure is repeated until the
resonant valley can be detected in the reflection of both
beams.

The drift in error voltage bias as displayed in Fig. 50,
continues to be a problem. It should be possible to use the
difference between the DC components of the detector outputs
as an error signal in a feedback control loop that would ad-
just the acousto-optic modulation amplitude to maintain con-
stant beam intensities. The drift in the beam intensities is
evident in Fig. 50. It is also clear that the cw beam inten-
sity varies more than the ccw beam. The cw beam is the beam
reflected from the surface of the beam-splitting pellicle,
and is thus affected by changes in the pellicle's position.
Any translation of the pellicle membrane affects the align-
ment and hence the finesse of the cw beam. To eliminate this

drift, either a more stable mount for the pellicle should be used, or the pellicle should be replaced by a beam-splitting cube.

By using the Rockwell "Zerodur" evacuated cavity, the cavity noise that plagued earlier experiments was virtually eliminated. However, the separate cw and ccw beam paths external to the cavity were very susceptible to noise. Any air current or dust particle passing through the beams introduced noise into the error signal. This fact was easily demonstrated by gently blowing air across one path. The separate reflecting mirrors and the reflecting membrane of the pellicle made the PRLG extremely susceptible to acoustic noise. The jumps in the error signal caused by acoustic noise appear as glitches on the strip recording of Fig. 50. The strip recorder had to be placed as far as possible from the PRLG so that the brush noise would not feedback into the error signal. Such sensitivity to the environment can be greatly reduced in the same way that cavity noise was reduced. All the components of the separate beam paths could be mounted in a solid piece of invar or ceramic which would then be partially evacuated.

The mode matching of both configurations can be improved. The poor mode match in the second configuration was largely due to deviations in lens focal lengths and improper placement. It would be beneficial to test the configuration of Appendix A as the mode matching lenses are of high quality, and the lens mount positions each lens to within one thou-

sandth of an inch of its desired position. The beam mode match
of this design should be precise, and allow the maximum trans-
mittance and minimum reflectance in the cavity.

The performance level attained for the PRLG in this ex-
periment is at par with performance levels attained with
active ring lasers. By improving the mode match, controlling
beam intensities, and isolating the beam paths from acoustic
noise, the performance of the PRLG can easily exceed the
levels of this experiment.

## Conclusions and Recommendations

The second configuration outperformed the first in this
experiment. Additionally the design of the second configura-
tion allowed the intensities of each beam path to be monitor-
ed. Because of the difference in mode matching techniques
between the two configurations, and a degree of mismatching
in both configurations, it would be beneficial to repeat the
design comparison using the mode matching optics displayed
in Appendix A. A circuit should also be constructed to equal-
ize the cw and ccw external beam intensities. Once the cir-
cuit is implemented and the beam intensities are equalized,
another drift measurment can be made to verify the postulate
that the bias drift in the PRLG was primarily due to drift
in external beam intensities. Although it is beyond the scope
of this thesis, the experimental results indicate that the
PRLG drift is much greater than the noise in the rate signal.
Therefore, future efforts to improve the performance of this

gyroscope should focus on eliminating the bias drift.

## VITA

Mark Eldon Nelson was born on 2 September 1953 in St. Louis, Missouri. He graduated from Parkway high school in Chesterfield, Missouri in 1971 and attended the USAF Academy from which he received the degree of Bachelor of Science in Electrical Engineering in June 1975. Upon graduation, he recieved a commission in the USAF. He completed navigator training and received his wings in April 1976. He then served as a navigator and instructor navigator in the 46th Air Refueling Squadron, K.I. Sawyer AFB, Michigan until entering the School of Engineering, Air Force Institute of Technology, in June 1982.

Permanent address: 726 Decker Lane
Creve Coeur, Missouri 63141

# Bibliography

1. Christiansen. "Ring Laser Gyro Technology, Its uses and Future." Meeting of the Institute of Navigation, Dayton Section. (May 1983).

2. Ezekiel, S. and Balsamo, S.R. "Passive Ring Resonator Laser Gyroscope," _Applied Physics Letters_, Vol 30, No9: 478-480. (May 1977).

3. Hecht, Eugene and Alfred Zajac. _Optics_. Reading: Addison Wesley Publishing Company, 1979.

4. Klein, Miles V. _Optics_. New York: John Wiley and Sons, 1970.

5. Kogelnik, H. and T. LI. "Laser Beams and Resonators," _Proceedings of the IEEE_, Vol 54:1312-1329. (October 1966).

6. Siegman, A. E. "Unstable Optical Resonators for Laser Applications," _Proceedings of the IEEE_, Vol 53:277-287 (March 1965).

7. Verdeyen, Joseph T. _Laser Electronics_. Englewood Cliffs: Prentice-Hall, Inc., 1981.

8. Yariv, Amnon. _Introduction to Optical Electronics_ (Second Edition). New York: Holt, Rinehart and Winston, 1976.
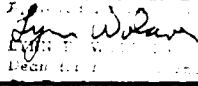
## Appendix A: Mode match Using Cylindrical Lenses

The third configuration uses the mode matching technique of Chapter II where each of the axes are matched independently using cylindrical lenses. In this case a Spectra-Physis frequency stabalized laser with a waist of .025 cm is matched to the cavity using a diverging lens with a focal length of -38.1 and two cylindrical lenses. One with a focal length of 69.2. The other with a focal length of 60. All focal lengths are in mm. All three lenses are broad-band anti-reflective coated. Reflection at normal incidence is less than 0.5%. The laser is placed 37.7 cm from the cavity input mirror. A stainless steel block bolts onto the front of the laser. The block acts as the lens mount for all three lenses. The diverging lens is mounted 1.8 cm from the laser face. The 60 mm cylindrical lens is mounted 4.29 cm from the laser face, and matches the x-axis radii of curvatures. The 69.2 mm cylindrical lens is mounted 5.16 cm from the laser face and matches the y-axis radii of curvatures. The solid stainless steel mount serves two purposes. First it positions each lens accuractly within one thousandth of an inch. Second it prevents the lenses from moving as independently as they would if they were independently mounted.

The mode match allows plenty of beam path to set up the PRLG in either of the design configurations tested in this thesis. The improvement in the mode match should improve the performance of both designs.

# REPORT DOCUMENTATION PAGE

| 1a. REPORT SECURITY CLASSIFICATION | | 1b. RESTRICTIVE MARKINGS | | |
|---|---|---|---|---|
| UNCLASSIFIED | | | | |
| 2a. SECURITY CLASSIFICATION AUTHORITY | | 3. DISTRIBUTION/AVAILABILITY OF REPORT | | |
| | | | | |
| 2b. DECLASSIFICATION/DOWNGRADING SCHEDULE | | Approved for public release; distribution unlimited. | | |
| 4. PERFORMING ORGANIZATION REPORT NUMBER(S) | | 5. MONITORING ORGANIZATION REPORT NUMBER(S) | | |
| AFIT/GEO/EE/ 83-3 | | | | |

| 6a. NAME OF PERFORMING ORGANIZATION | 6b. OFFICE SYMBOL (If applicable) | 7a. NAME OF MONITORING ORGANIZATION |
|---|---|---|
| School of Enginnering | AFIT/ENG | |

| 6c. ADDRESS (City, State and ZIP Code) | 7b. ADDRESS (City, State and ZIP Code) |
|---|---|
| Air Force Institute of Technology Wright-Patterson AFB, Ohio 45433 | |

| 8a. NAME OF FUNDING/SPONSORING ORGANIZATION | 8b. OFFICE SYMBOL (If applicable) | 9. PROCUREMENT INSTRUMENT IDENTIFICATION NUMBER |
|---|---|---|
| | | |

| 8c. ADDRESS (City, State and ZIP Code) | 10. SOURCE OF FUNDING NOS. | | | |
|---|---|---|---|---|
| | PROGRAM ELEMENT NO. | PROJECT NO. | TASK NO. | WORK UNIT NO. |
| | | | | |

11. TITLE (Include Security Classification)
See Box 19

12. PERSONAL AUTHOR(S)
Mark E. Nelson, B.S., Capt, USAF

| 13a. TYPE OF REPORT | 13b. TIME COVERED | | 14. DATE OF REPORT (Yr., Mo., Day) | 15. PAGE COUNT |
|---|---|---|---|---|
| MS Thesis | FROM _____ TO _____ | | 1983 December | 95 |

16. SUPPLEMENTARY NOTATION

| 17. COSATI CODE | | | 18. SUBJECT TERMS (Continue on reverse if necessary and identify by block number) |
|---|---|---|---|
| FIELD | GROUP | SUB. GR. | LASER, RING LASER, GYROSCOPE, RESONANT CAVITY |
| 01 | 04 | | |
| 20 | 05 | | |

19. ABSTRACT (Continue on reverse if necessary and identify by block number)

Title: IMPLEMENTATION AND EVALUATION OF TWO DESIGN CONCEPTS
OF THE PASSIVE RING RESONATOR LASER GYROSCOPE

Thesis Chairman: Salvatore R. Balsamo, Major, USAF

| 20. DISTRIBUTION/AVAILABILITY OF ABSTRACT | 21. ABSTRACT SECURITY CLASSIFICATION | |
|---|---|---|
| UNCLASSIFIED/UNLIMITED ☒ SAME AS RPT. ☐ DTIC USERS ☐ | UNCLASSIFIED | |
| 22a. NAME OF RESPONSIBLE INDIVIDUAL | 22b. TELEPHONE NUMBER (Include Area Code) | 22c. OFFICE SYMBOL |
| Salvatore R. Balsamo, Major, USAF | 303-259-3506 | FJSRL/USAFA |

Two configurations of the passive resonant ring laser gyroscope were evaluated. The first configuration detected cavity resonance by monitoring the beams transmitted through the cavity. The second configuration detected resonance by monitoring the beams reflected from the cavity input mirrors. The resonant cavity of both configurations had a rated finesse of 9800. making the gyro much more sensitive than earlier versions. Additionally, much of the cavity moise that plagued earlier experiments was eliminated by mounting the cavity mirrors on a solid ceramic block, and evacuating the beam paths.

Alignment data indicated that the signal strength in the reflected beam had six times the power of the signal in the transmitted beam. However, the bias on the reflected signal was seven times the signal strength. This bias intensity increased the shot noise in the detector circuit.

Rotation was simulated in the gyro by shifting beam frequencies. Th strength of the error signal was calibrated to angular rotation. Asignal to noise ratio of one was then converted to a noise equivalent rotation. Using a 100 second integration time, the noise equivalent rotation of the first configuration was twelve milli-earthrate, and four milli-earthrate for the second configuration. The detection of resonance using the reflected beam increased sensitivity threefold.

END